PERMEABILITY TESTING OF SHEARED FRACTURES IN SANDSTONES

Panupong Suanprom

A Thesis Submitted in Partial Fulfillment of the Requirements

for the Degree of Master of Engineering in Geotechonolgy

Suranaree University of Technology

Academic Year 2009

การทดสอบความซึมผ่านของรอยแตกในหินทรายภายใต้แรงเฉือน

นายภานุพงศ์ สวนพรหม

วิทยานิพนธ์นี้เป็นส่วนหนึ่งของการศึกษาตามหลักสูตรปริญญาวิศวกรรมศาสตรมหาบัณฑิต
สาขาวิชาเทคโนโลยีธรณี
มหาวิทยาลัยเทคโนโลยีสุรนารี
ปีการศึกษา 2552

PERMEABILITY TESTING OF SHEARED

FRACTURES IN SANDSTONES

Suranaree University of Technology has approved this thesis submitted in partial fulfillment of the requirements for a Master's Degree.

Thesis Examining Committee

_____

(Asst. Prof. Thara Lekuthai)

Chairperson

_____

(Assoc. Prof. Dr. Kittitep Fuenkajorn)

Member (Thesis Advisor)

_____

(Dr. Prachya Tepnarong)

Member

_____ _____

(Prof. Dr. Pairote Sattayatham) (Assoc. Prof. Dr. Vorapot Khompis)

Acting Vice Rector for Academic Affairs Dean of Institute of Engineering

ภานุพงศ์ สวนพรหม : การทดสอบความซึมผ่านของรอยแตกในหินทรายภายใต้แรงเฉือน (PERMEABILITY TESTING OF SHEARED FRACTURES IN SANDSTONES) อาจารย์ที่ปรึกษา : รองศาสตราจารย์ ดร.กิตติเทพ เฟื่องขจร, 78 หน้า.

น้ำบาดาลในมวลหินเป็นปัจจัยสำคัญประการหนึ่งที่ควบคุมเสถียรภาพเชิงกลศาสตร์ของความลาดชัน เหมืองใต้ดิน และอุโมงค์ ความซึมผ่านของมวลหินจะมีทิศทางซึ่งถูกควบคุมด้วยระบบของรอยแตกเพราะหินทั่วไปจะมีค่าความซึมผ่านค่อนข้างต่ำ สำหรับมวลหินในธรรมชาติที่ไม่มีการขุดเจาะมาเกี่ยวข้องนั้นคุณลักษณะของรอยแตกจะเป็นตัวกำหนดปริมาณและทิศทางการไหลของน้ำซึ่งสามารถวัดได้จากการทดสอบในภาคสนามและบางครั้งมีการคำนวณด้วยแบบจำลองเข้ามาประกอบด้วย การตัดความลาดชันและขุดเจาะอุโมงค์จะรบกวนสภาวะของมวลหินโดยรอบและมีการเปลี่ยนแปลงค่าความเค้นบนรอยแตกและบ่อยครั้งจะทำให้มีการเคลื่อนตัวของรอยแตกด้วย ดังนั้นโครงสร้างวิศวกรรมดังกล่าวมักจะเพิ่มค่าความซึมผ่านของมวลหินซึ่งบางครั้งอาจเพิ่มขึ้นหลายเท่า ถึงแม้ผลกระทบดังกล่าวได้มีการกล่าวถึงมาเป็นเวลาช้านาน การศึกษาค่าความซึมผ่านของรอยแตกในหินที่มีผลกระทบจากการเคลื่อนตัวแบบเฉือนยังมีน้อยมาก

วัตถุประสงค์ของงานวิจัยนี้คือเพื่อศึกษาค่าความซึมผ่านของรอยแตกในหินทรายภายใต้ความเค้นในแนวตั้งและความเค้นเฉือนซึ่งจะมีการทดสอบการไหลของน้ำด้วยวิธีอัดน้ำด้วยแรงดันแบบผันแปร โดยใช้รอยแตกที่ทำขึ้นในห้องปฏิบัติการของหินทราย 4 ชนิด หินทรายดังกล่าวคือ หินทรายชุดภูพาน ชุดเสาขรัว ชุดภูกระดึง และชุดพระวิหาร ซึ่งอยู่ในกลุ่มหมวดหินโคราช จะมีการวัดการเปลี่ยนแปลงของรอยเปิดเผยอ อัตราการไหลของน้ำ และค่าความเค้นเฉือนที่เปลี่ยนไป ซึ่งจะนำมาใช้ในการคำนวณการเปลี่ยนแปลงของค่าความซึมผ่านในรอยแตกในฟังก์ชั่นของการเคลื่อนตัวในแนวเฉือน ผลที่ได้ระบุว่าการเปิดเผยอเชิงกายภาพและเชิงไฮดรอลิกจะเพิ่มขึ้นตามการเคลื่อนตัวแบบเฉือนซึ่งจะเห็นได้ชัดสำหรับรอยแตกที่อยู่ภายใต้ความเค้นตั้งสูง ความซึมผ่านของรอยแตกภายใต้สภาวะที่ไม่มีแรงเฉือนและสภาวะที่มีแรงเฉือนสูงสุดจะมีค่าใกล้เคียงกัน การเปิดเผยอเชิงกายภาพจะมีค่ามากกว่าการเปิดเผยอเชิงไฮดรอลิก 5-10 เท่า ส่งผลให้ค่าความซึมผ่านเชิงกายภาพสูงกว่าค่าความซึมผ่านเชิงไฮดรอลิก 10-100 เท่า ซึ่งสามารถอธิบายได้โดยการเปิดเผยอเชิงกายภาพไม่ได้พิจารณาผลกระทบของความขรุขระของรอยแตกที่เป็นปัจจัยทำให้ระยะทางของการไหลของน้ำยาวขึ้น ผลต่างระหว่างค่าความซึมผ่านภายใต้ความเค้นสูงสุด

และภายใต้ความเค้นคงเหลือจะมีค่าสูงขึ้นเมื่อความเค้นตั้งฉากบนรอยแตกนั้นมีค่ามากขึ้น ค่าความซึมผ่านของรอยแตกจะลดลงเมื่อความเค้นในแนวตั้งมีค่าสูงขึ้น ค่าความซึมผ่านของ หินทรายที่ทดสอบได้จากงานวิจัยนี้มีค่าระหว่าง 0.1×10^{-3} เมตร/วินาที ถึง 10×10^{-3} เมตร/วินาที

สาขาวิชา เทคโนโลยีธรณี ลายมือชื่อนักศึกษา _____

ปีการศึกษา 2552 ลายมือชื่ออาจารย์ที่ปรึกษา _____

PANUPONG SUANPROM : PERMEABILITY TESTING OF SHEARED FRACTURES IN SANDSTONES. THESIS ADVISOR : ASSOC. PROF. KITTITEP FUENKAJORN, Ph.D., PE., 78 PP.

PERMEABILITY/FRACTURE/APERTURE/SHEAR STRESS

Groundwater in rock mass is one of the key factors governing the mechanical stability of slope embankments, underground mines and tunnels. Permeability of rock mass is path dependent, controlling mainly by the system of fractures as the permeability of the intact rocks is normally low. For undisturbed rock mass (before excavation) the joint characteristics that dictate the amount and direction of water flow, can be adequately determined by means of in-situ measurements, and sometimes assisted by numerical modeling. Slope or underground excavations disturb the surrounding rock mass, alter the stress states on the fracture planes, and often cause relative displacements of the rock fractures. In most cases the excavations usually increase the surrounding rock mass permeability and sometimes by several orders of magnitude. Even though this effect has long been recognized, specific study on the rock fracture permeability as affected by the shearing displacement has been rare.

The objective of this research is to experimentally assess the permeability of sandstone fractures under normal and shear stresses. The effort primarily involves performing series of falling head flow tests on tension-induced fractures in four types of sandstone samples. The tested sandstones belong to the Phu Phan, Sao Khua, Phu Kradung and Pra Wihan formations of the Khorat group. The changes of the physical and hydraulic apertures, the water flow rates, and the applied shear stresses are

monitored and used to calculate the changes of the fracture permeability as a function of shear displacement. The results indicate that the physical aperture e_p and hydraulic aperture e_h increase with shearing displacement, particularly under high normal stresses. The magnitudes of fracture permeability under no shear and under peak shear stress are similar. For both peak and residual regions, the physical apertures are about 5 to 10 times greater than the hydraulic apertures, as a result the fracture hydraulic conductivity determined from the physical aperture are about one to two orders of magnitudes greater than these determined from the equivalent hydraulic apertures. This is probably because the measured physical apertures do not consider the effect of fracture roughness that causes a longer flow path. The difference between the permeability under residual shear stress and that under peak stress becomes larger under higher normal stresses. The fracture hydraulic conductivities exponentially decrease with increasing the normal stresses. Their permeability is in the range between 0.1×10^{-3} m/s and 10×10^{-3} m/s.

School of Geotechnology Student's Signature _____

Academic Year 2009 Advisor's Signature _____

ACKNOWLEDGEMENTS

The author wishes to acknowledge the support from the Suranaree University of Technology (SUT) who has provided funding for this research.

Grateful thanks and appreciation are given to Assoc. Prof. Dr. Kittitep Fuenkajorn, thesis advisor, who lets the author work independently, but gave a critical review of this research. Many thanks are also extended to Asst. Prof. Thara Lekuthai and Dr. Prachaya Tepnarong, who served on the thesis committee and commented on the manuscript.

Finally, I most gratefully acknowledge my parents and friends for all their supported throughout the period of this research.

Panupong Suanprom

TABLE OF CONTENTS

Page

TABLE OF CONTENTS (Continued)

Page

LIST OF TABLES

Table **Page**

LIST OF FIGURES

Figure **Page**

LIST OF FIGURES (Continued)

Figure **Page**

LIST OF FIGURES (Continued)

Figure **Page**

LIST OF FIGURES (Continued)

Figure **Page**

LIST OF SYMBOLS AND ABBREVIATIONS

c	=	Cohesion
e_h	=	Hydraulic aperture
e_m	=	Mechanical aperture
e_p	=	Physical aperture
H_1, H_2	=	Excess pressure head at beginning and end of test
JCS	=	Joint compressive strength
JRC	=	Joint roughness coefficient
K_h	=	Hydraulic conductivity
K_m	=	Hydraulic conductivity (determined from mechanical aperture)
K_p	=	Hydraulic conductivity (determined from physical aperture)
k_n	=	Joint normal stiffness
k_s	=	Joint shear stiffness
R	=	Radius of flow path
R^2	=	Coefficient of determination
r	=	Radius of injection hole
r_b	=	Pipette radius
t_1, t_2	=	Time at beginning and end of test
α_p	=	Empirical constant for equation (4.6)
α_r	=	Empirical constant for equation (4.7)
β_p	=	Empirical constant for equation (4.6)

LIST OF SYMBOLS AND ABBREVIATIONS (Continued)

β_r	=	Empirical constant for equation (4.7)
δ_n	=	Normal displacement
δ_s	=	Shear displacement
ϕ_p	=	Peak friction angle
ϕ_r	=	Residual friction angle
γ	=	Unit weight of water
μ	=	Dynamic viscosity
σ_c	=	Uniaxial compressive strength
σ_n	=	Normal stress
τ	=	Shear stress
τ_p	=	Peak shear strength
τ_r	=	Residual shear strength

CHAPTER I

INTRODUCTION

1.1 Background of problems and significance of the study

Groundwater in rock mass is one of the key factors governing the mechanical stability of slope embankments, underground mines and tunnels. The lack of proper understanding of the water pressure and flow characteristics in rock mass makes it difficult to predict the water inflow in underground mines and tunnels under the complex hydro-geological environments. Unlike those in the soil mass, permeability of rock mass is path dependent, controlling mainly by the system of fractures as the permeability of the intact rocks is normally low. For undisturbed rock mass (before excavation) the joint characteristics (e.g., roughness, aperture, spacing and orientation) that dictate the amount and direction of water flow, can be adequately determined by means of in-situ measurements, and sometimes assisted by numerical modeling. Slope or underground excavations disturb the surrounding rock mass, alter the stress states on the fracture planes, and often cause relative displacements of the rock fractures. In most cases the excavations usually increase the surrounding rock mass permeability and sometimes by several orders of magnitude. Even though this effect has long been recognized, specific study on the rock fracture permeability as affected by the shearing displacement has been rare.

1.2 Research objectives

The objective of this research is to experimentally assess the permeability of rock fractures under shearing displacements. The effort primarily involves performing a series falling head tests on tension-induced fractures in four types of sandstone samples. The rocks belong to the Phu Phan, Sao Khua, Phu Kradung and Pra Wihan formations of the Khorat group. They expose in the north and northeast of Thailand and have impacts on mechanical stability of many engineering structures in the region. The changes of the physical and hydraulic apertures, the water flow rates, and the applied shear stresses will be monitored and used to calculate the changes of the fracture permeability as a function of shear displacement.

1.3 Research methodology

As shown in figure 1.1, the research methodology comprises 5 steps; literature review, sample collection and preparation, flow testing, development of mathematical relations and flow equations, and discussions and conclusions.

1.3.1 Literature review

Literature review is carried out to study the genesis and classification of fractures, permeability of rock mass, apertures, and stress effects on fracture void geometry. The sources of information are from text books, journals, technical reports and conference papers. A summary of the literature review is given in the thesis.

1.3.2 Sample collection and preparation

Sandstone samples are collected from the site. A minimum of 4 sandstone types are collected. Sample preparation is carried out in the laboratory at the Suranaree University of Technology. Samples for the falling head test are

prepared to have fractures area of about 10×10 square centimeters. The fractures are artificially made in the laboratory by tension inducing method.

1.3.3 Falling head flow testing

Falling head tests are conducted by injecting water into the center hole of rectangular blocks of sandstone. A fracture is created across the block specimen either by saw-cutting or tension inducing methods. The 8 mm hole is drilled into the upper block of the sample to allow water flow through the fracture. Then the pair of tested sandstone blocks are placed in the shear box of the direct shear testing machine. The shear force is applied while the flow testing is continued. The constant normal stresses on the fracture are varied from 1 to 5 MPa by using loading devices.

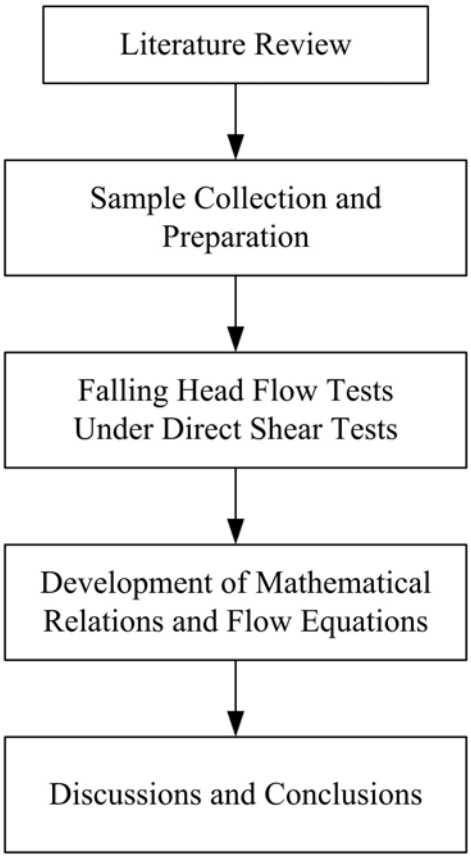

Figure 1.1 Research methodology

The test is terminated when a total of 10 mm of shear displacement is reached. A minimum of 6 samples for each rock type will be tested.

1.3.4 Development of mathematical relations and flow equations

Results from laboratory measurements in terms of rock fracture permeability, fractures aperture, stress states and shear displacement are used to formulate mathematical relations.

1.3.5 Conclusion and thesis writing

All research activities, methods, and results are documented and complied in the thesis.

1.4 Scope and limitations of the study

The scope and limitations of the research include as follows.

1. Laboratory experiments are conducted on specimens from four types of sandstone, including the Sao Khua, Phu Kradung, Pra Wihan, and Phu Phan formations.

2. Testing on fractures is made under normal stresses ranging from 1 to 5 MPa

3. All tested fractures are artificially made in the laboratory.

4. Fracture permeability is determined by falling head flow testing.

5. All tests are conducted under ambient temperature.

6. Up to 6 samples are tested for each rock type.

7. The test fractures area is 10×10 square centimeters.

8. Water is used as flow medium.

9. No field testing is conducted.

10. X-ray diffraction analysis are performed to determine the mineral compositions of the tested rocks.

1.5 Thesis contents

Chapter I introduces the thesis by briefly describing the background of problems and significance of the study. The research objectives, methodology, scope and limitations are identified. **Chapter II** summarizes results of the literature review. **Chapter III** describes the sample preparation and laboratory experiment. **Chapter IV** presents the results obtained from the laboratory testing. **Chapter V** concludes the research results, and provides recommendations for future research studies. **Appendix A** provides detailed results of direct shear testing. **Appendix B** provides detailed of technical publication.

CHAPTER II

LITERATURE REVIEW

2.1 Introduction

This chapter summarizes the results of literature review carried out to improve an understanding of simulation of rock slope failure using physical model. The topics reviewed here include the fluid flow in fracture rock, permeability of fracture rock, and stiffness of fracture.

2.2 Literature review

Pyrak-Noltea and Morrisa (2000) stated that fracture specific stiffness and fluid flow through a single fracture under normal stress are implicitly related through the geometry of the void space and contact area that comprise the fracture. Data from thirteen difference rock samples, each containing a single fracture, show that relationships between fracture specific stiffness and fluid flow through a fracture fall into two general classes of behavior. Fractures either fall on a loosely-defined universal curve relating fluid flow to fracture specific stiffness, or else the flow is weakly dependent on fracture specific stiffness. The second relationship shows that flow decreases slowly with increasing fracture specific stiffness. The first relationship shows that flow decreases rapidly for increases in fracture specific stiffness. To understand this behavior, computer simulations on simulated single fractures were performed to calculate fluid flow, fracture displacement, and fracture specific stiffness as a function of normal stress. Simulated fractures with spatially

correlated and uncorrelated aperture distributions were studied. Fractures with spatially uncorrelated aperture distributions tend to exhibit a weak dependence of fluid flow on fracture specific stiffness because these fractures tend to have multiple connected paths across the sample which can support flow with uniformly distributed contact area. Thus an increment in stress will increase the stiffness of the fracture without greatly reducing the amount of fluid flow. On the other hand, fractures with spatially correlated aperture distributions tend to belong to the universal relationship because correlated fractures tend to have only one or two dominant flow paths and the contact area is limited to a few regions resulting in a compliant fracture. Thus an increment in stress on a spatially correlated fracture will result in an increase in stiffness and rapid decrease in fluid flow. These spatial correlations in fracture void geometry can be differentiated in the laboratory based on the observed fracture specific stiffness-fluid flow relationship for a single fracture under normal loading.

Lee and Cho (2002) built a hydro-mechanical testing system, which is capable of measuring both the flow rates and the normal and shear displacement of a rock fracture, was built to investigate the hydraulic behavior of rough tension fractures. Laboratory hydraulic tests in linear flow were conducted on rough rock fractures, artificially created using a splitter under various normal and shear loading. Prior to the tests, aperture distributions were determined by measuring the topography of upper and lower fracture surfaces using a laser profilometer. Experimental variograms of the initial aperture distributions were classified into four groups of geostatistical model, though the overall experimental variograms could be well fitted to the exponential model. The permeability of the rough rock fractures decayed exponentially with respect to the normal stress increase up to 5 MPa. Hydraulic

behaviors during monotonic shear loading were significantly affected by the dilation occurring until the shear stress reached the peak strength. With the further dilation, the permeability of the rough fracture specimens increased more. However, beyond shear displacement of about 7 to 8 mm, permeability gradually reached a maximum threshold value. The combined effects of both asperity degradation and gouge production, which prohibited the subsequent enlargement of mean fracture aperture, mainly caused this phenomenon. Permeability changes during cyclic shear loading showed somewhat irregular variations, especially after the first shear loading cycle, due to the complex interaction from asperity degradations and production of gouge materials. The relation between hydraulic and mechanical apertures was analyzed to investigate the valid range of mechanical apertures to be applied to the cubic law.

Seidel and Haberfield (2002) have conducted an investigation into the behavior of rock joints subjected to direct shear. Both concrete/rock and rock/rock joints were investigated. The behavior of rock/rock joints is important for the assessment of stability issues involving rock masses (e.g. rock slope stability). Concrete/rock joints are vital to the assessment of performance of concrete piles socketed into rock, rock anchors and concrete dam foundations. This investigation included an extensive series of direct shear tests under a range of stress boundary conditions. The rock used for the tests was a soft artificial siltstone, called Johnstone. The results from the tests on concrete/Johnstone joints have been presented on Johnstone/Johnstone joints in Fleuter (MEngSc Dissertation, Department of Civil Engineering, Monash University, Australia, 1997) and Pearce (Ph.D. dissertation, Department of Civil Engineering, Monash University, Australia, 2001, in preparation). This paper describes the theoretical models developed to simulate the

observed behavior, including asperity sliding, asperity shearing, post-peak behavior, asperity deformation and distribution of stresses on the interface. These models have been combined into a micro-mechanical simulation of joint shear.

Jiang et al. (2004) stated that evaluations of shear strength and flow behavior of rock joints play an important role in designing of deep underground openings and in performing underground waster disposal risk assessments. Although shear strength and flow behavior can be investigated in a laboratory using a direct shear apparatus, the experimental results are influenced by boundary conditions and the simulation conditions may not be representative of the field conditions. They introduce a newly developed automated servo-control hydro-mechanical direct shear apparatus that is capable of automatically adjusting the normal stiffness according to the deformational capacity of the surrounding rock masses, thereby accurately simulating the high pressure head in deep underground locations. The proposed apparatus was used to perform shear tests on artificial joint specimens. Experimental measurements of the coupled mechanical and hydraulic behavior of rock joints under CNL and CNS conditions were analyzed. The shear strength and permeability results exhibited a regular variation due to the interaction of the joint roughness and gouge production. The rock joint permeability results can be applied to deep underground construction.

Son et al. (2004) proposed a new constitutive model for the shear behavior of rough rock joints. Within the framework of the classical elasto-plastic theories, the model incorporates the dilation and surface degradation which are distinct features of rough rock joints. The elastic behavior is represented by the shear and normal stiffness. To calculate the plastic displacements after yielding, the non-associated flow rule is applied. Maksimovic's equation and Lee's empirical formula for joint

shear strength are used for yield and plastic potential functions. The changes of the joint roughness angle that occurred in pre- and post-peak ranges of shear strength curve were approximated by simple power expressions of accumulated tangential plastic work. A joint finite element, which has 6-node and zero thickness, was used for implementing the proposed joint constitutive model. In order to evaluate the performance of the model, numerical direct shear tests were carried out. The results of the simulation confirmed that the proposed model could reproduce salient phenomena commonly observed in actual shear test of rock joints, including the shear strength hardening, softening, and dilation phenomena.

Hamiel et al. (2005) stated that the dilation of rock under shear gives rise to detectable effects both in laboratory experiments and in field observations. Such effects include hardening due to reduction in pore pressure and asymmetrical distribution of deformation following strike slip earthquakes. They examine the nonlinear poroelastic behavior of isotropic rocks by a new model that integrates Biot's classic poroelastic formulation together with nonlinear elasticity, and apply it to Coulomb failure criterion and pore pressure response to a fault slip. They investigate the poroelastic response of two alternative forms of a non-Hookean secondorder term incorporated in the poroelastic energy. This term couples the volumetric deformation with shear strain. Like linear poroelasticity, our model shows an increase of pore pressure with mean stress (according to Skempton coefficient B) under undrained conditions. In addition, in their model pore pressure varies also with deviatoric stresses, where rising deviatoric stresses (at constant mean stress) decreases pore pressure (according to Skempton coefficient A), due to dilatancy. The first version of our model is consistent with a constant A smaller than 1/3, which is in

agreement with the classic work of Skempton, but does not fit well the measured undrained response of sandstones. The second model allows A and B to vary with shear stress, and displays the experimentally observed connection between pore pressure and deviatoric stresses under undrained conditions in Berea and Navajo sandstone samples. Numerical results predict dilatancy hardening and suggest that it should be taken into consideration in Coulomb failure stress calculations. They apply our model to the distribution of pore pressure changes in response to a fault slip. Results of numerical simulations of coseismic deformation demonstrate that due to dilatancy regions of decreasing pore pressure are larger relative to regions of increasing pore pressure. The model predictions have significant implications for coseismic water level changes and post-seismic pore pressure diffusion and crustal deformation.

Auradou et al. (2006) investigated the effect on the transport properties of a fracture of a shear displacement u between its complementary surfaces experimentally and numerically. The shear displacement u induces an anisotropy of the fracture aperture field with a correlation length scaling of $|u|$, which is significantly larger in the direction perpendicular to u. This reflects the presence of long fluid flow channels perpendicular to the shear displacement, resulting in a higher effective permeability in that direction. Such channels will have a strong influence on the transport characteristics of a fracture, such as, for instance, its thermal exchange area, crucial for geothermal applications. Miscible displacement fronts in shear-displaced fractures obtained experimentally display a self-affine geometry with a characteristic exponent directly related to that of the fracture surfaces. They present a simple model, based on the channeling of the aperture field, which reproduces the

front geometry when the mean flow is parallel to the channels created by the shear displacement

Baghbanan and Jing (2006) investigated permeability of fractured rocks considering the correlation between distributed fracture aperture and trace length, based on a newly developed correlation equation. The influence of the second moment of the lognormal distribution of apertures on the existence of representative elementary volume (REV), and the possibility of equivalent permeability tensor of the fractured rock mass, is examined by simulating flow through a large number of stochastic discrete fracture network (DFN) models of varying sizes and varying fracture properties. The REV size of the DFN models increases with the increase of the second moment of the lognormal distribution, for both the correlated and uncorrelated cases. The variation of overall permeability between different stochastic realizations is an order of magnitude larger when the aperture and length are correlated than when they are uncorrelated. The mean square error of the directional permeability increases with increasing value of the second moment of the lognormal distribution function, and good fitting to an ellipsis of permeability tensor can only be reached with very large sizes of DFN models, compared with the case of constant fracture aperture, regardless of fracture trace length.

Baghbanan and Jing (2008) studied the effect of stress on permeability and fluid flow patterns in fractured rock masses when distributed fracture aperture is correlated with fracture trace length, using a discrete element method (DEM). The basic assumptions are that the rock matrix is impermeable and linearly elastic, and that the fluid flows only in fractures. The results show that when small stress ratios (K = horizontal/vertical stress) are applied at the model boundaries, the overall

permeability of the fracture network is generally decreased. However, contribution from a few large fractures of higher hydraulic conductivity prevents drastic reduction of the overall permeability, compared with models that assume uniform fracture apertures. With large values of the stress ratio, both the overall permeability and flow patterns are controlled by a combination of highly conductive larger fractures and fractures with shear slipping and dilation, with much increased overall permeability and shear-induced flow channeling. These results show significant difference between correlated and non-correlated aperture and fracture length distributions, and highlight more significant scale andstress dependence of hydro-mechanical behavior of fractures rocks when geometric parameters of rock fractures are correlated.

Giacominia et al. (2008) investigated the flow anisotropy within a natural joint subjected to mechanical shear. The cubic law is the simplest way to describe fluid flow through rock joints but because of rock wall roughness, deviations from this model have been observed. The Reynolds equation usually gives better results. In this study, micro-scale roughness is taken into account to define a reduced coefficient of permeability. Numerical simulations have been carried out by applying Darcy's law to the rock joint, described as an equivalent porous medium. The numerical simulations are based on experimental data obtained by Hans (PhD, Grenoble, 2002) from a series of hydromechanical shear tests on a rock joint replica. The numerical results have been compared to the experimental ones, and to the results obtained by applying the Reynolds equation, to assess the relevance of the simulations. For the fracture studied, the approach proposed herein can reproduce relatively well the experimental flow anisotropy, and provides consistent values of flow rates, whereas the Reynolds equation tends to give higher flow rates.

Jiang et al. (2009) built a new method for determination of fracture normal stiffness is developed in this paper. From the point of hydro-mechanical coupling, the relationship between transmissivity and depth is utilized to calculate fracture normal stiffness of large-scale rock masses, which is an important but difficult-to-obtain parameter. The basic idea is that flow in fractured media is very sensitive to aperture of discontinuity, and the aperture of the discontinuity is mainly determined by the normal stress and normal stiffness. A decrease in transmissivity of fractured rock masses with increasing depth, as indicated in hydraulic tests, is due to closure of the joints caused by an increase in the normal stress that is nearly proportional to depth. Consequently, it is possible to estimate in-situ fracture normal stiffness by using information of depth-dependent transmissivity. An equation is derived to achieve the purpose. In our preliminary case study at the fractured sandstone on the left bank of the Xiaolangdi Reservoir in China, the variable fracture normal stiffness is estimated. It satisfies the fact that normal stiffness will increase with increasing stress, i.e. with increasing depth. The value obtained by our method is of the same order of magnitude as the normal stiffness values obtained from laboratory tests reported in the literature. Furthermore, the estimated deformation modulus of the rock mass is close enough to that obtained from in-situ tests or inverse analysis

CHAPTER III

SAMPLE PREPARATION

3.1 Introduction

The tested sandstones are from four sources: Phu Phan, Phra Wihan, Phu Kradung and Sao Kua formations (hereafter designated as PP, PW, PK and SK sandstones) (Figure 3.1). They belong to the Khorat group and widely expose in the north and northeast of Thailand. They also have significant impacts on stability of many engineering structures constructed in the regions (e.g., slope embankments, underground mines and tunnels).

3.2 Sample preparation

A minimum of 4 sandstone types are prepared. Sample preparation is carried out in the laboratory at the Suranaree University of Technology. Samples for the falling head test are prepared to have fractures area of about 10×10 square centimeters. The fractures are artificially made by applying a line load to induce a splitting tensile crack in 10×10×12 cm^3 prismatic blocks of PW, PP, PK and SK sandstones (Figure 3.2). The injection hole at the center of the lower block is 0.8 cm in diameter. Up to 6 samples have been prepared for each rock type. Their roughness is observed and classified by comparing with a reference profiles given by Barton (joint roughness coefficient – JRC, Barton, 1973).

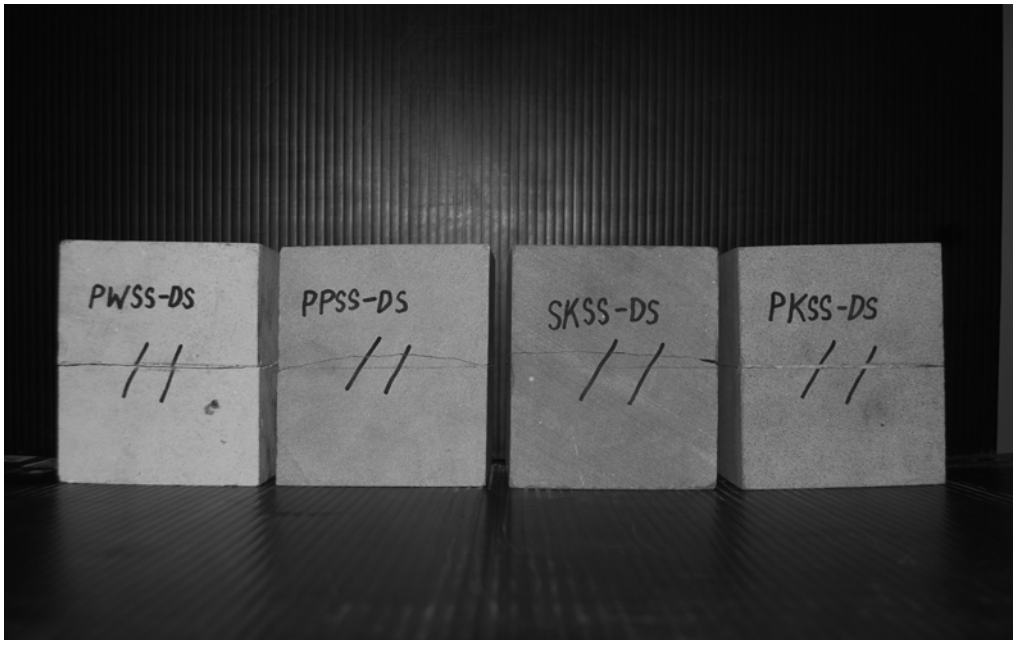

Figure 3.1 Some sandstone specimens prepared for falling head test under normal and shear stresses.

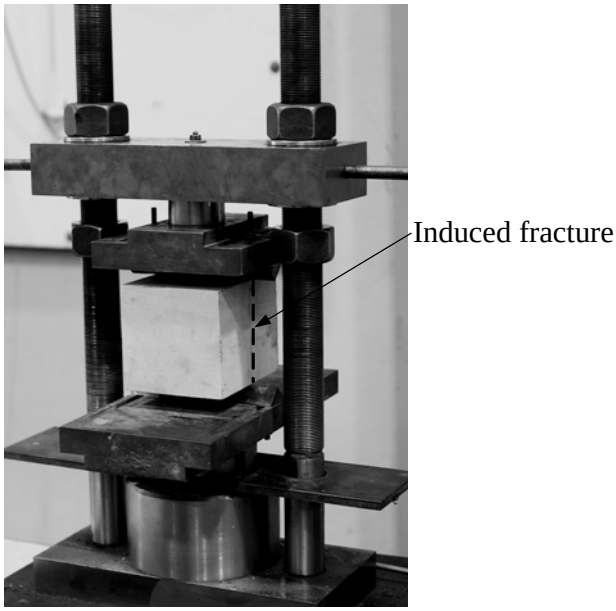

Figure 3.2 A 10×10×12 cm^3 block of PW sandstone is line-loaded to induce tensile fracture in mid-length of the block.

3.3 Mineralogical study

X-ray diffraction analyses are performed to determine rock mineral compositions. Table 3.1 summarizes the results. These fine-grained quartz sandstones are selected for this study primarily because they have highly uniform texture, grain size and density.

Table 3.1 Mineral compositions of tested sandstones obtained from X-ray diffraction.

Rocks	Density (g/cc)	Grain Size (mm)	Mineral Compositions				
			Quartz (%)	Albite (%)	Kaolinite (%)	Feldspar (%)	Mica (%)
PW	2.35	1.5-2.0	99.47	-	0.53	-	-
PP	2.45	1.5-2.0	98.40	-	-	-	1.60
PK	2.63	0.1-1.5	48.80	46.10	5.10	-	-
SK	2.37	0.1-1.0	57.00	39.50	-	2.90	0.60

CHAPTER IV

LABORATORY TESTING

4.1 Introduction

The objective of the laboratory testing is to determine the permeability of rock fractures under shearing stresses and displacements. This chapter describes the method and results. The changes of the physical and hydraulic apertures, the water flow rates, and the applied shear stresses are monitored and used to calculate the changes of the fracture permeability as a function of shear displacement.

4.2 Test method

Falling head flow tests (Freeze and Cherry, 1979) have been performed to determine the fracture permeability of sandstone specimens under shear stresses. Series of direct shear tests are performed on the specimens with the tension-induced fractures (Figures 4.1 through 4.3). The sample preparation and test procedure follow the applicable ASTM standard (ASTM 5607-95) and the ISRM suggested method (Brown, 1981), as mush as practical. The maximum water head above the tested fracture is 1.23 m. The injection hole at the center of the lower block is 0.8 cm in diameter. The fractures are artificially made by applying a line load to induce a splitting tensile crack in $10\times10\times12$ cm^3 prismatic blocks of sandstones. The fracture area is 10×10 cm^2. The constant normal stresses are 0.69, 1.38, 2.76, 3.45 and 4.14. MPa. The shear stress is applied using model No. SBEL DR440 while the shear

displacement and head drop are monitored for every 0.5 mm increment of shear displacement. The maximum shear displacement is 10 mm. The (physical) fracture aperture is physically measured before and after normal and shear stress applications. The fracture dilations are also monitored during the shear test.

The physical, mechanical and hydraulic apertures are determined and used to calculate the hydraulic conductivity of the tested fractures. The physical aperture (e_p) is obtained from the actual measurements of the fractures before and during normal and shear stress applications. The measurement points are at the four corners of the shear box. The physical aperture at each shear displacement is an average from the four measurements. The mechanical aperture (e_m) in mm is calculated by (Barton and Bakhtar, 1983 and Bandis et al., 1983, 1985):

$$e_m = [JRC/5] [0.2(\sigma_c/JCS) - 0.1] \quad (4.1)$$

where σ_c and JCS are the uniaxial compressive strength and joint compressive strength of the rock in MPa. Here σ_c and JCS are assumed to be equal.

The equivalent hydraulic aperture (e_h) for radial flow is calculated by (Maini, 1971):

$$e_h = [[\ln(H_1 / H_2) r_b^2 \ln(R / r) 6\mu] / [(t_2 - t_1)\gamma]]^{1/3} \quad (4.2)$$

where γ is the unit weight of water (N/m^2), μ is the dynamic viscosity ($N \cdot s/m^2$), H_1 and H_2 are the water heads at t_1 and t_2, r_b is the pipette radius (m), R is the radius of flow path (m), and r is the radius of the injection hole (m).

The fracture permeability is calculated by (Zeigler, 1976):

$$K = \gamma e^2 / 12\mu \quad (4.3)$$

where K represents hydraulic conductivity between smooth and parallel plates and e is the parallel plate aperture. It is assumed here that the flow is isotropic across the fracture plane, and that the intact rock is impermeable.

Here the fracture conductivity is calculated for three types of fracture apertures: e_p, e_m and e_h, and differentiated by different symbols as K_p – physical, K_m – mechanical, and K_h – hydraulic conductivities.

Their roughness is observed and classified by comparing with a reference profiles given by Barton (joint roughness coefficient – JRC, Barton, 1973). The measured JRC values range from 11, 13 to 15, which are classified as rough and undulating; bedding and tectonic joints; and relief joints, respectively. From equation (4.1) the equivalent mechanical apertures for the above JRC values are 220, 260 and 300 micro-meters.

The joint shear stiffness for various normal stresses is calculated at the 50% peak stress using an equation (Indraratna and Ranjith, 2001):

$$k_s = \tau_s/\delta_s \quad (4.4)$$

where k_s is the joint shear stiffness (MPa/m), τ_s is the shear stress (MPa), δ_s is the shear displacement (m).

The normal stiffness of fractured is calculated by (Indraratna and Ranjith, 2001):

$$K_n = \sigma_n/\delta_n \quad (4.5)$$

where k_n is the joint normal stiffness (MPa/m), τ_n is the normal stress (MPa), δ_n is the normal displacement (m).

Table 4.1 summarizes the results of the fracture stiffness calculations for PW, PP, PK and SK sandstones. The fracture stiffness determined here compare well with these obtained by (Pyrak-Nolte et al., 2000). The joint shear stiffness tends to increase with the normal stresses.

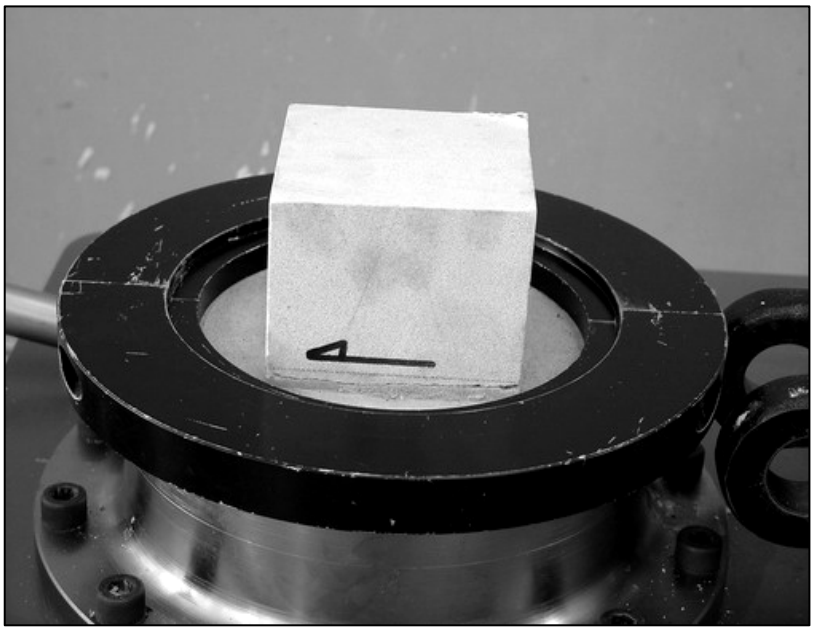

Figure 4.1 Direct shear strength test on tension induced joint in PW specimen with 10x10 cm of contact area.

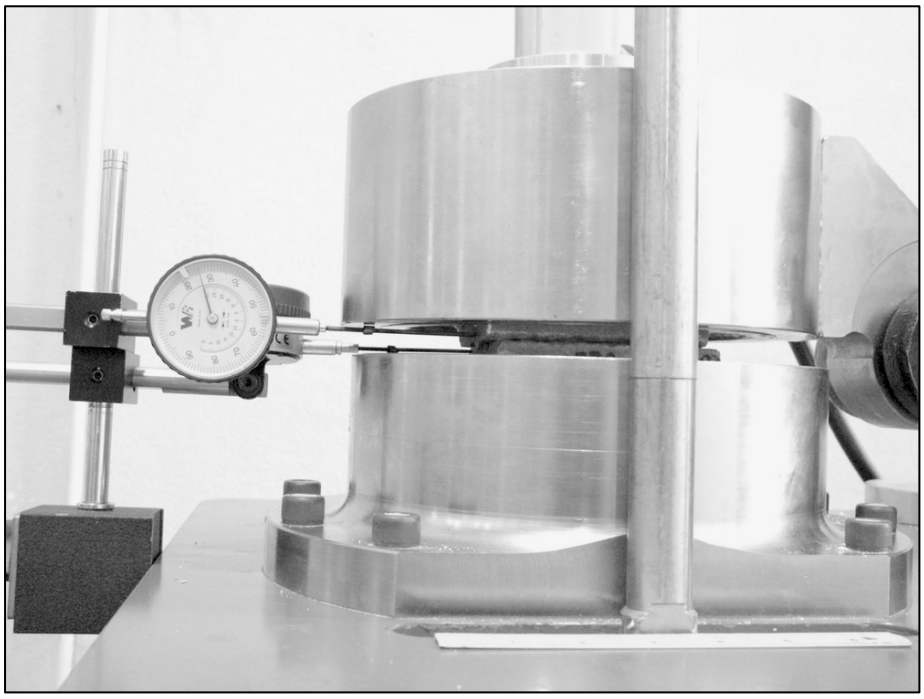

Figure 4.2 Upper block of PP sandstone specimen are attached with displacement dial gages during shear testing.

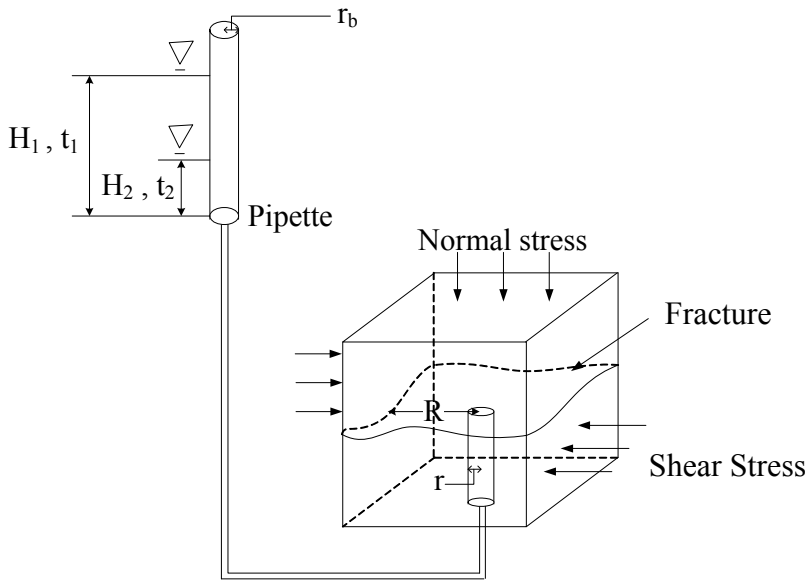

Figure 4.3 Laboratory arrangement for falling head test under normal and shear stresses.

Table 4.1 Normal and shear stiffness of sandstone.

Specimen No.	σ_n (MPa)	K_s (GPa/m)	K_n (GPa/m)
PWSS-DS-02	0.69	12.5	1.86
PWSS-DS-04	1.38	13.33	4.18
PWSS-DS-03	2.07	14.29	4.27
PWSS-DS-01	2.76	15.38	8.36
PWSS-DS-06	3.49	16.67	4.42
PWSS-DS-05	4.14	18.18	4.16
Average		15.06±2.12	4.54±2.1
PPSS-DS-01	0.69	5.26	5.31
PPSS-DS-02	1.38	6.67	6.57
PPSS-DS-06	2.07	8.7	4.81
PPSS-DS-04	2.76	10	10.13
PPSS-DS-05	3.49	11.76	6.07
PPSS-DS-03	4.14	14.29	8.72
Average		9.45±3.31	6.94±2.07
PKSS-DS-01	0.69	4.65	3.14
PKSS-DS-02	1.38	5.4	3.25
PKSS-DS-03	2.07	9.09	3.87
PKSS-DS-04	2.76	12.5	4.8
PKSS-DS-05	3.49	16.67	7.35
PKSS-DS-06	4.14	18.18	6.49
Average		11.08±5.68	4.82±1.75
SKSS-DS-01	0.69	5	1.15
SKSS-DS-02	1.38	7.14	3.29
SKSS-DS-03	2.07	10	7.53
SKSS-DS-04	2.76	12.5	6.42
SKSS-DS-05	3.49	16.67	7.35
SKSS-DS-06	4.14	18.18	7.02
Average		11.58±5.21	5.46±2.63

4.3 Test results

The fracture hydraulic conductivities are calculated for the three aperture measurements and plotted as a function of shear displacement (u) for normal stresses (σ_n) of 0.69, 2.75 and 4.14 MPa in Figures 4.4 through 4.7 for PW, PP, PK and SK sandstones. They are also compared with their corresponding shear stress-shear displacement diagram (τ-δ_s).

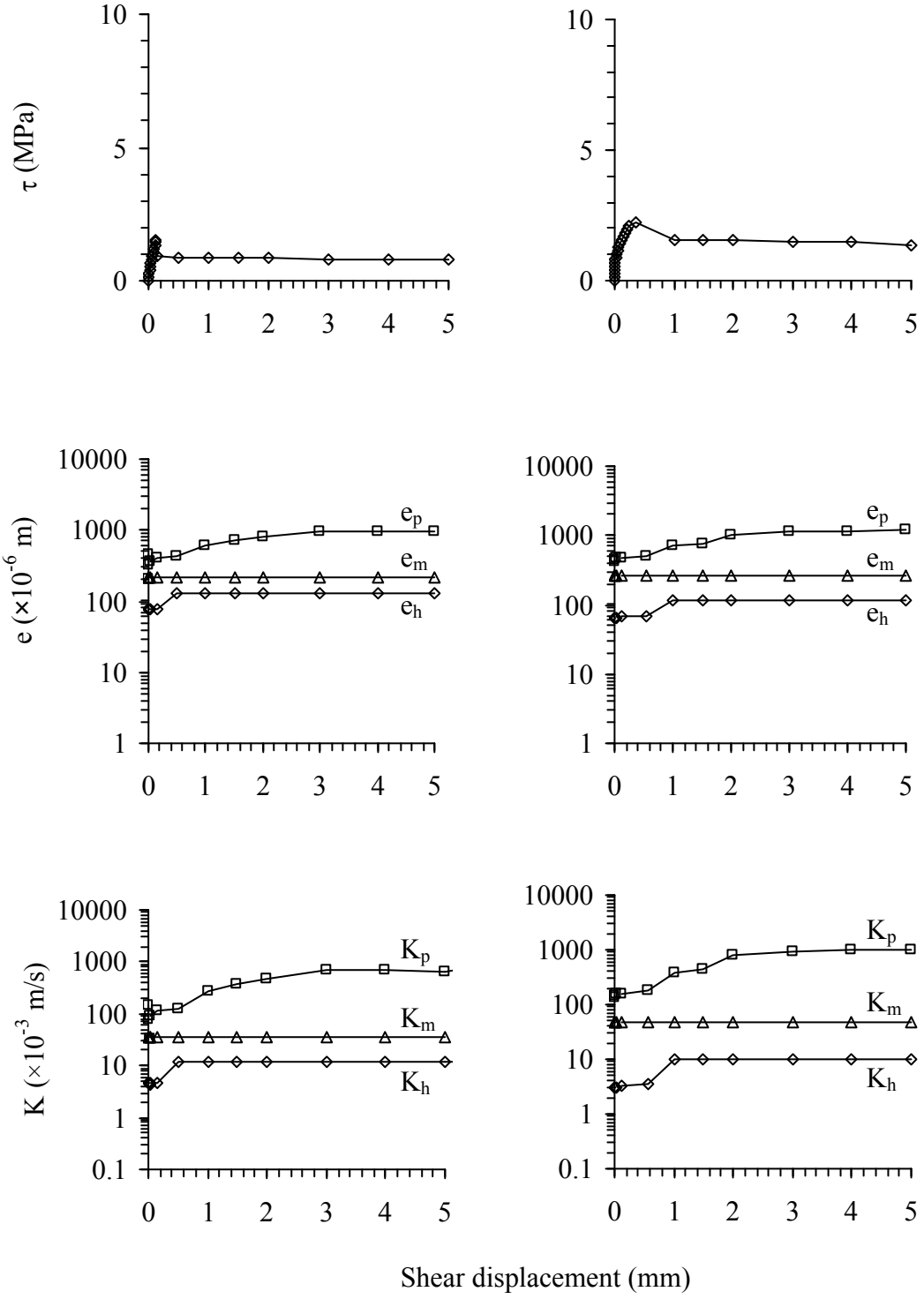

Figure 4.4(a) Shear stress, fracture aperture, and hydraulic conductivity as a function of shear displacement (δ_s) at normal stress = 0.69 MPa (left) and 1.38 MPa (right) for PW sandstone.

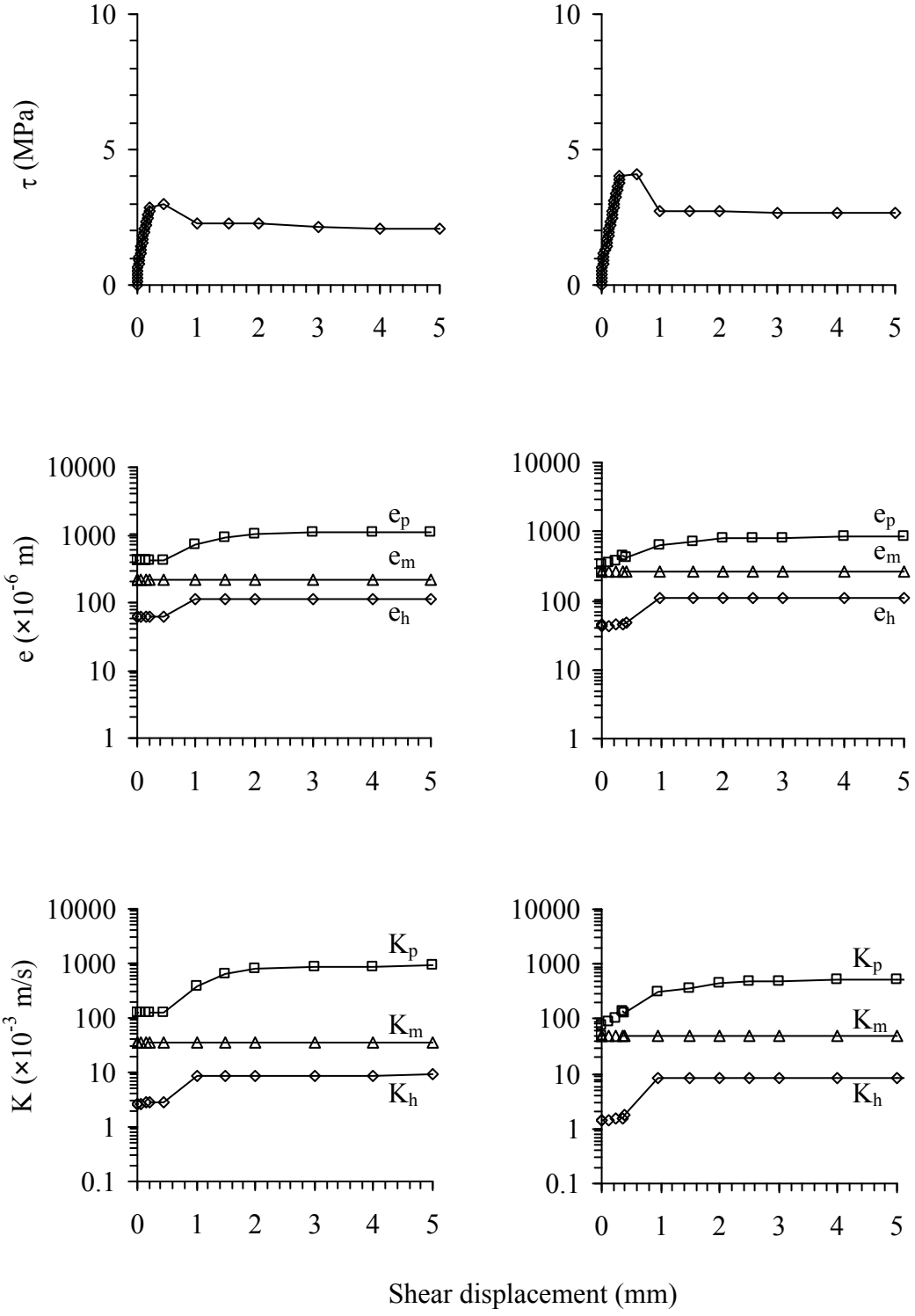

Figure 4.4(b) Shear stress, fracture aperture and hydraulic conductivity as a function of shear displacement (δ_s) at normal stress = 2.07 MPa (left) and 2.76 MPa (right) for PW sandstone.

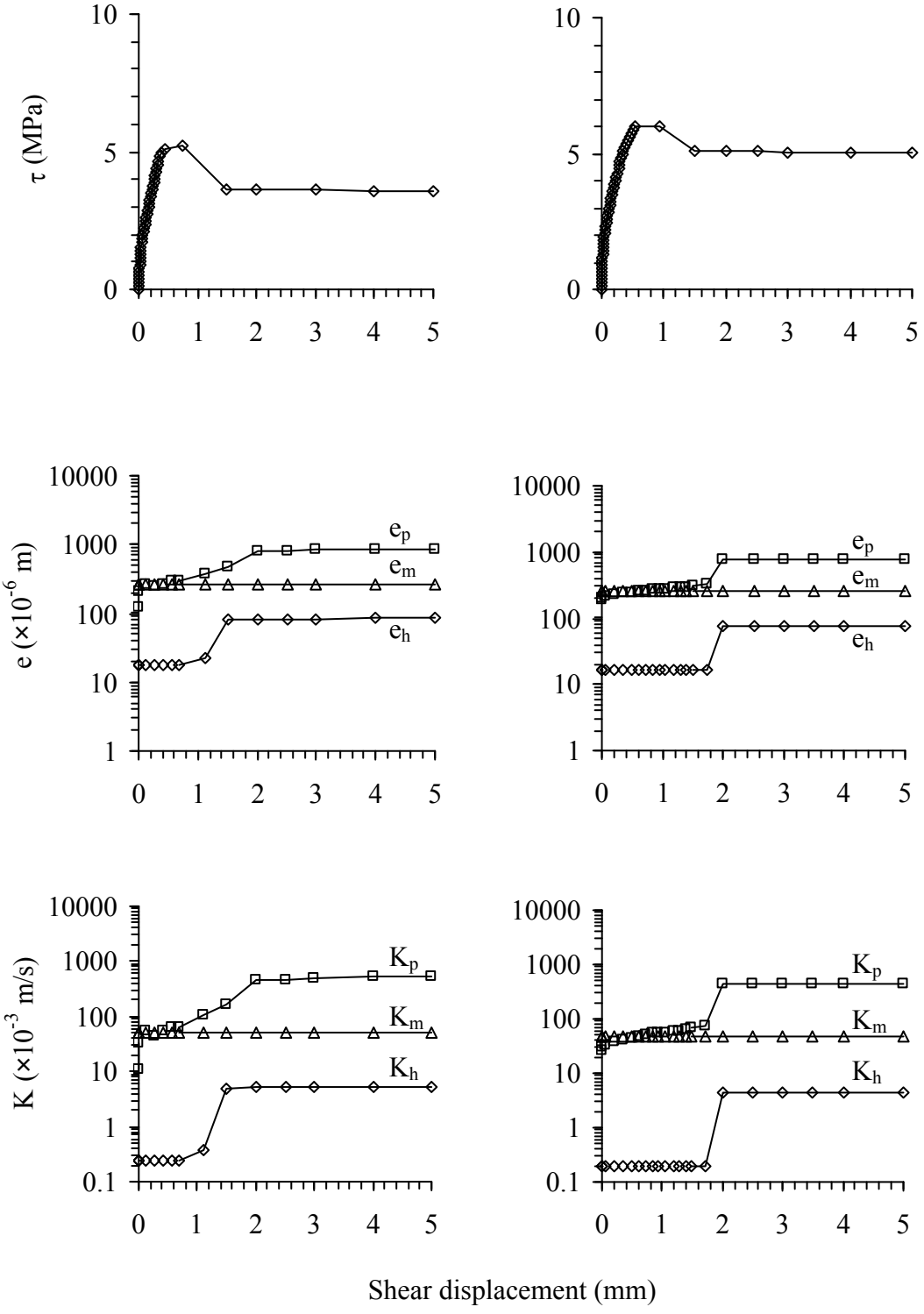

Figure 4.4(c) Shear stress, fracture aperture and hydraulic conductivity as a function of shear displacement (δ_s) at normal stress = 3.49 MPa (left) and 4.14 MPa (right) for PW sandstone.

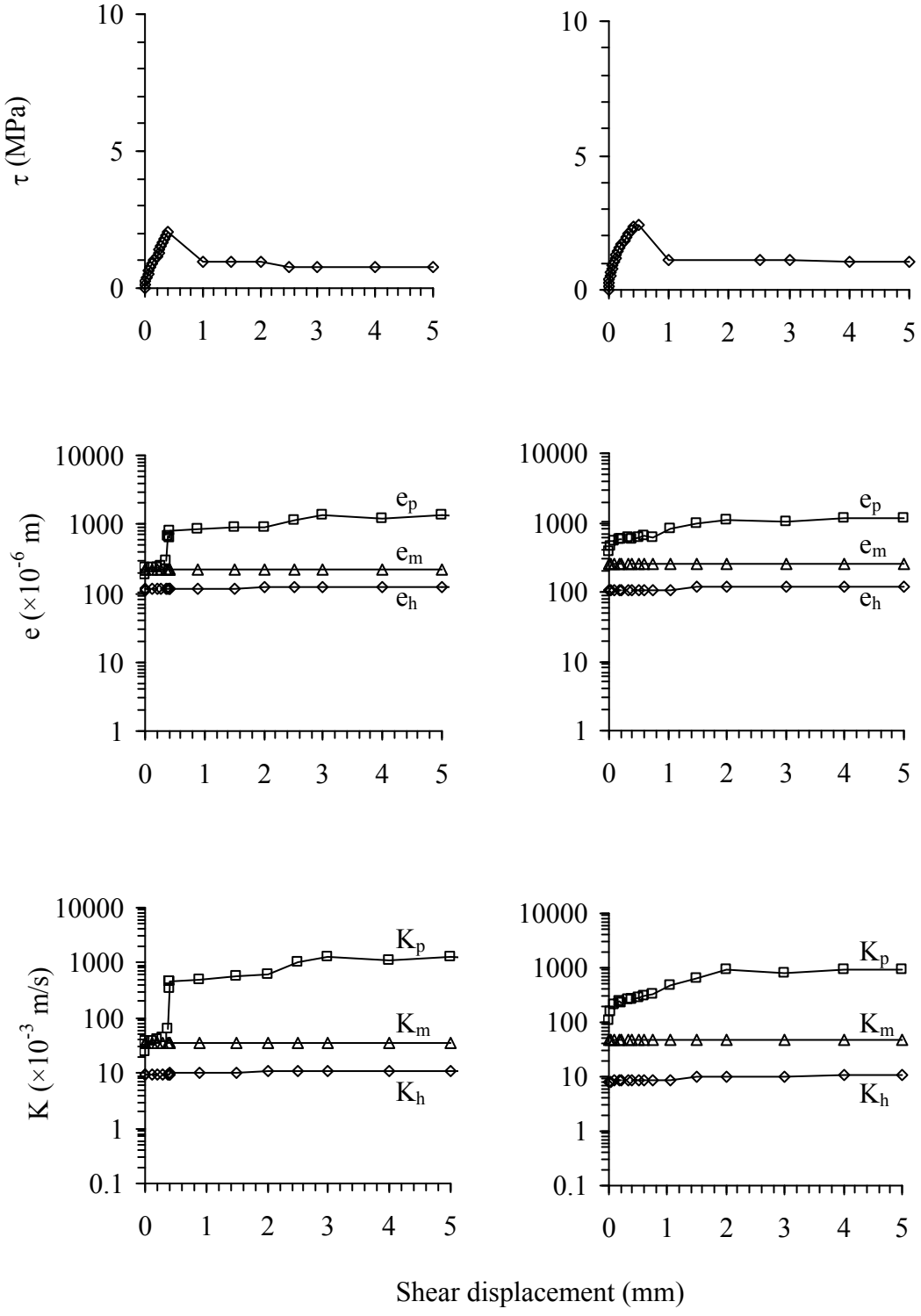

Figure 4.5(a) Shear stress, fracture aperture and hydraulic conductivity as a function of shear displacement (δ_s) at normal stress = 0.69 MPa (left) and 1.38 MPa (right) for PP sandstone.

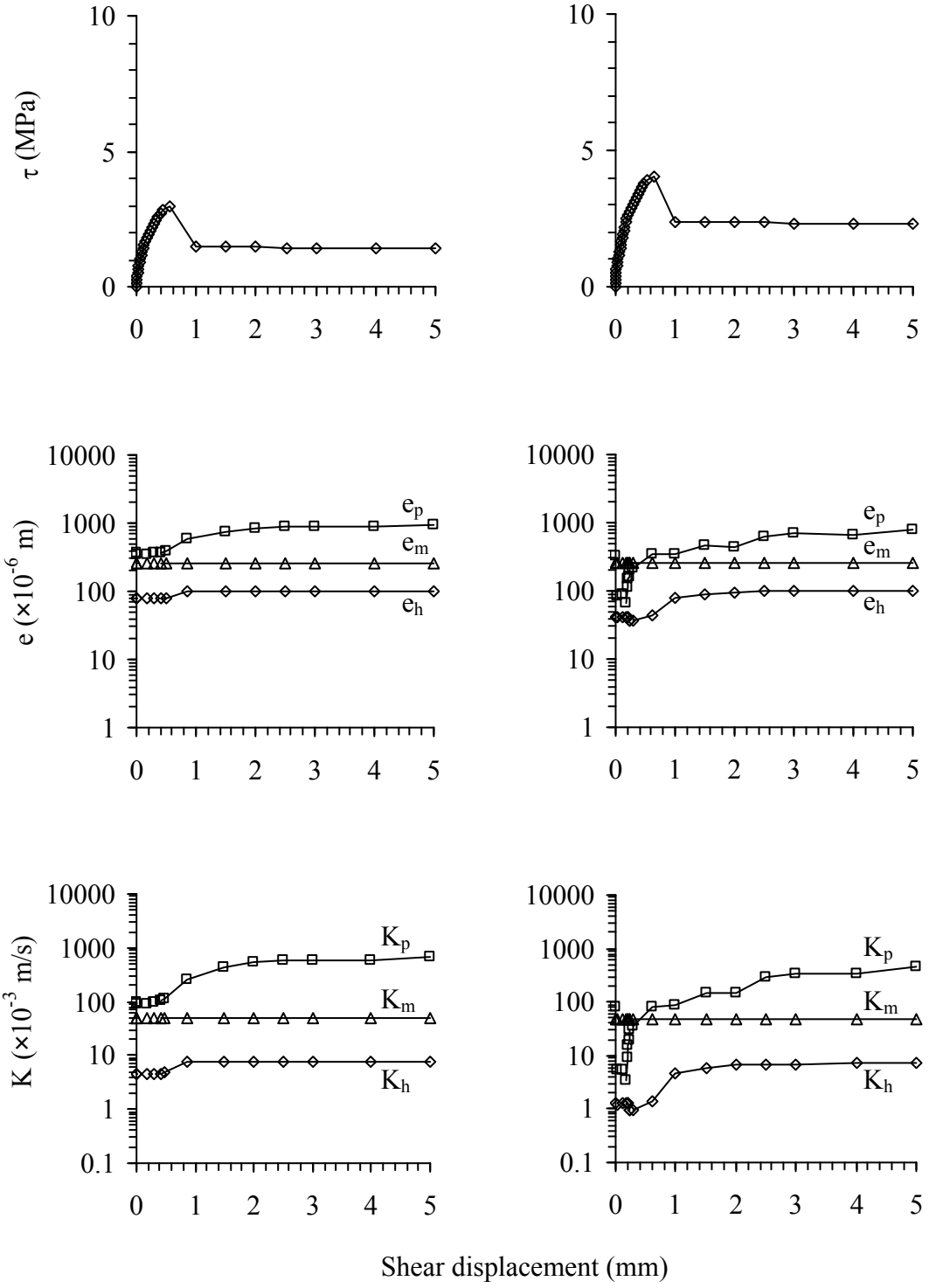

Figure 4.5(b) Shear stress, fracture aperture and hydraulic conductivity as a function of shear displacement (δ_s) at normal stress = 2.07 MPa (left) and 2.76 MPa (right) for PP sandstone.

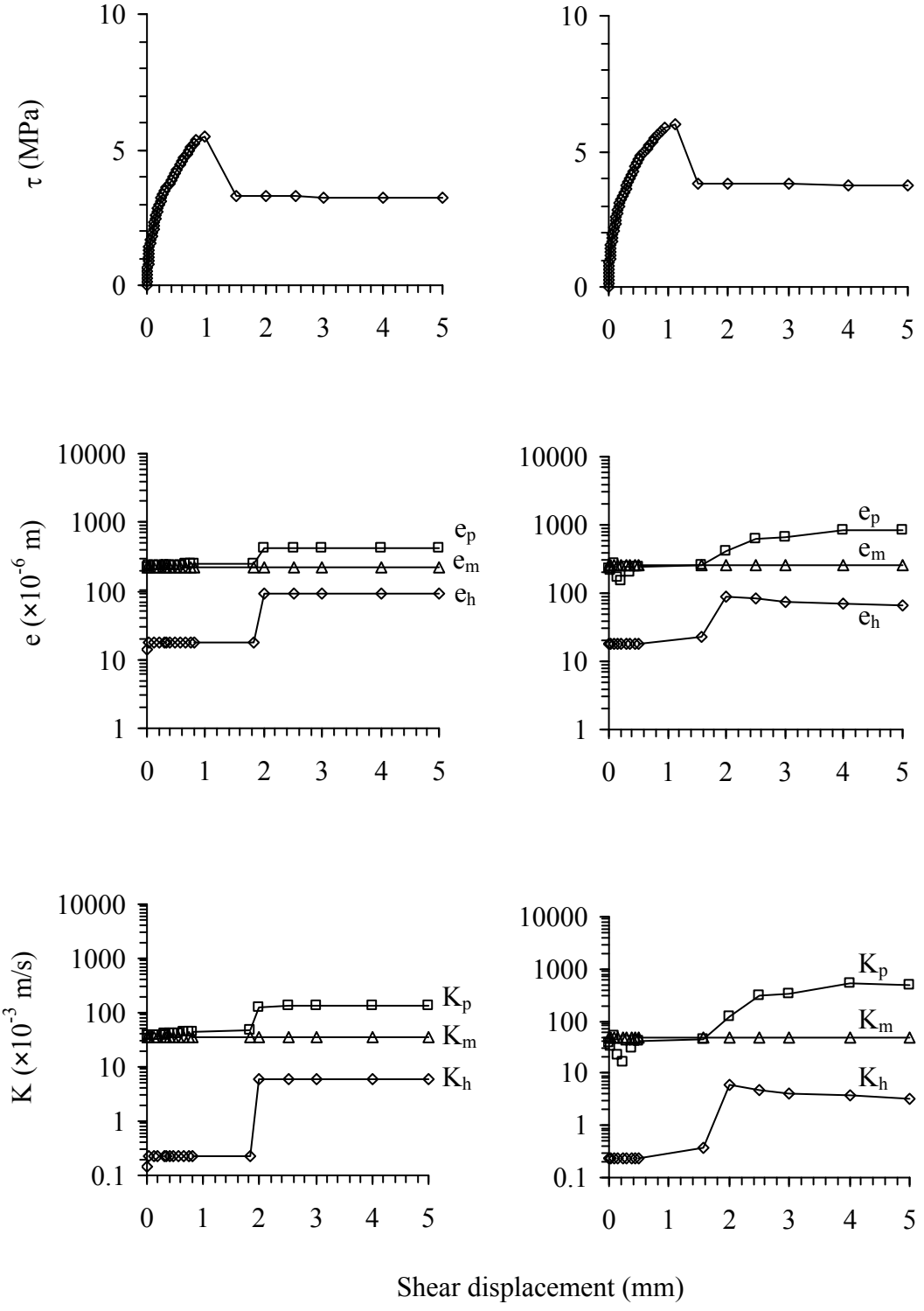

Figure 4.5(c) Shear stress, fracture aperture and hydraulic conductivity as a function of shear displacement (δ_s) at normal stress = 3.49 MPa (left) and 4.14 MPa (right) for PP sandstone.

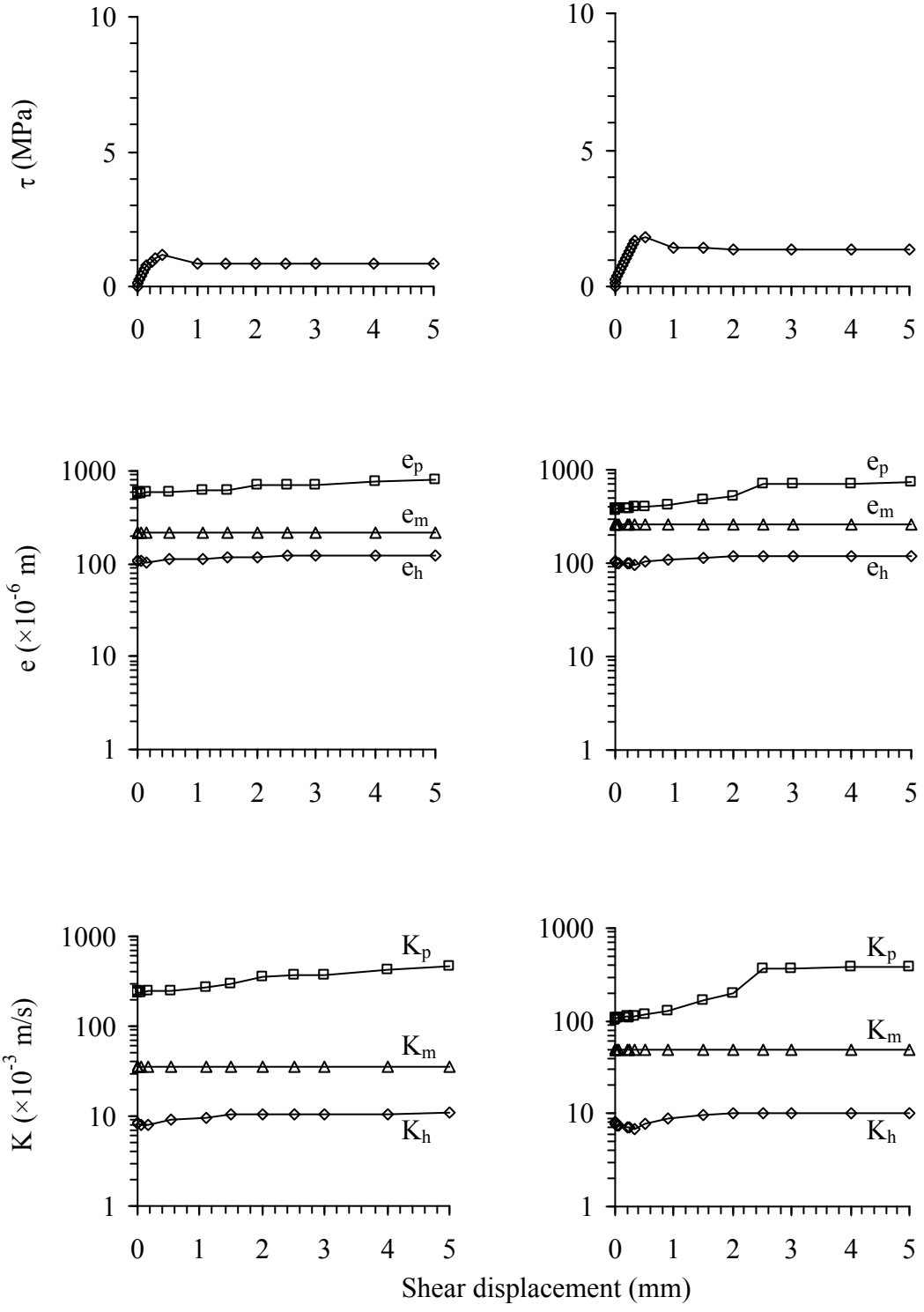

Figure 4.6(a) Shear stress, fracture aperture and hydraulic conductivity as a function of shear displacement (δ_s) at normal stress = 0.69 MPa (left) and 1.38 MPa (right) for PK sandstone.

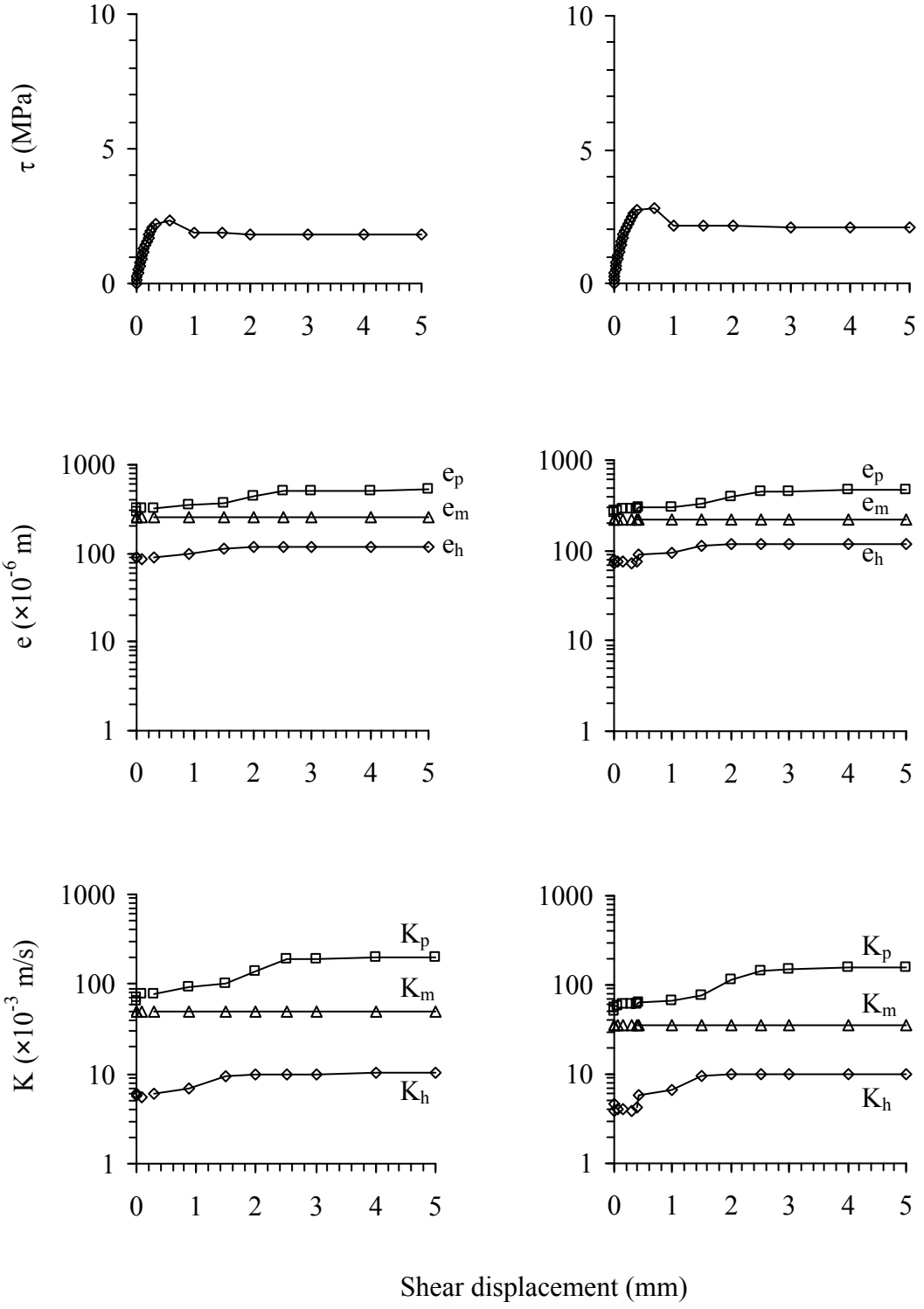

Figure 4.6(b) Shear stress, fracture aperture and hydraulic conductivity as a function of shear displacement (δ_s) at normal stress = 2.07 MPa (left) and 2.76 MPa (right) for PK sandstone.

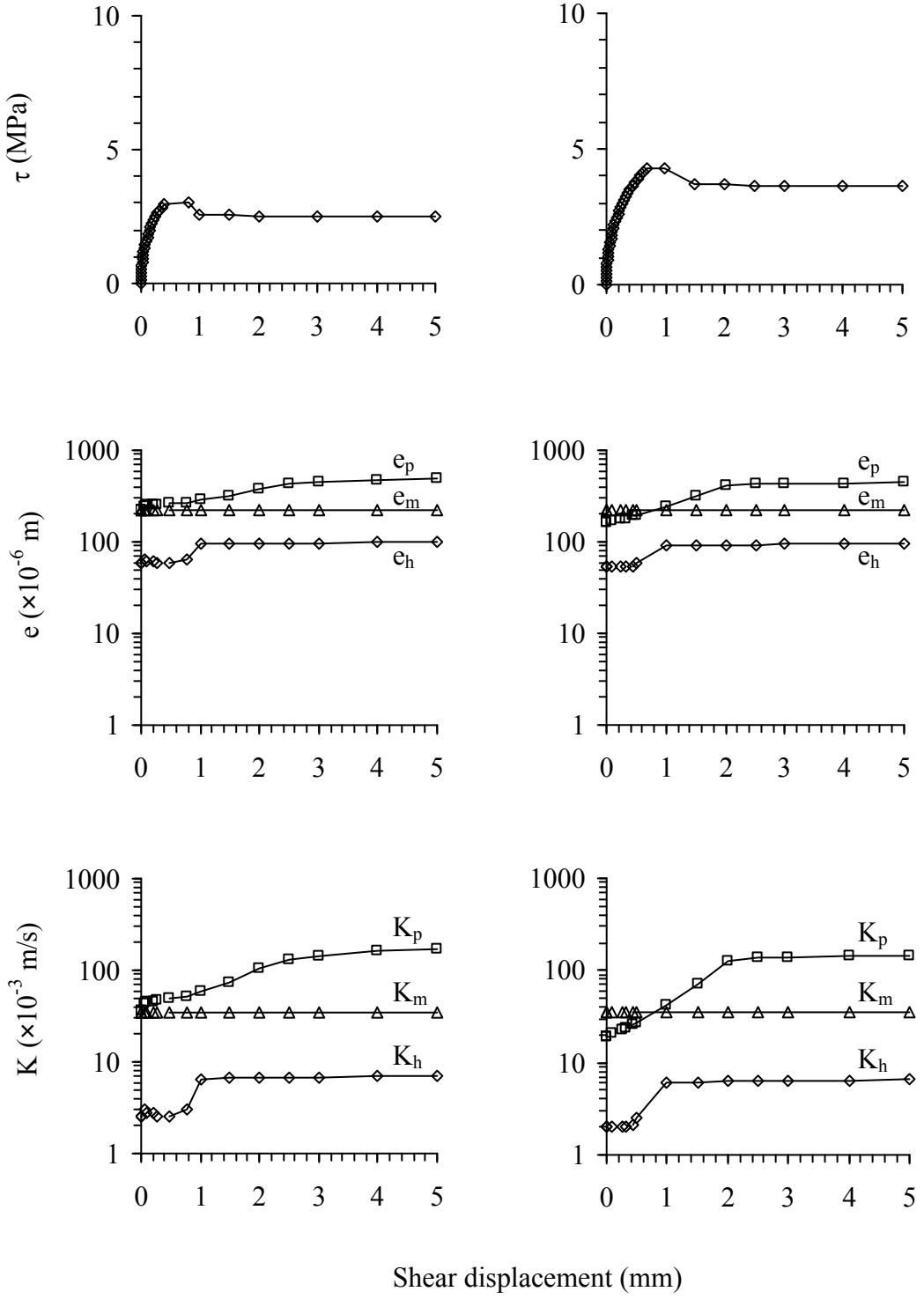

Figure 4.6(c) Shear stress, fracture aperture and hydraulic conductivity as a function of shear displacement (δ_s) at normal stress = 3.49 MPa (left) and 4.14 MPa (right) for PK sandstone.

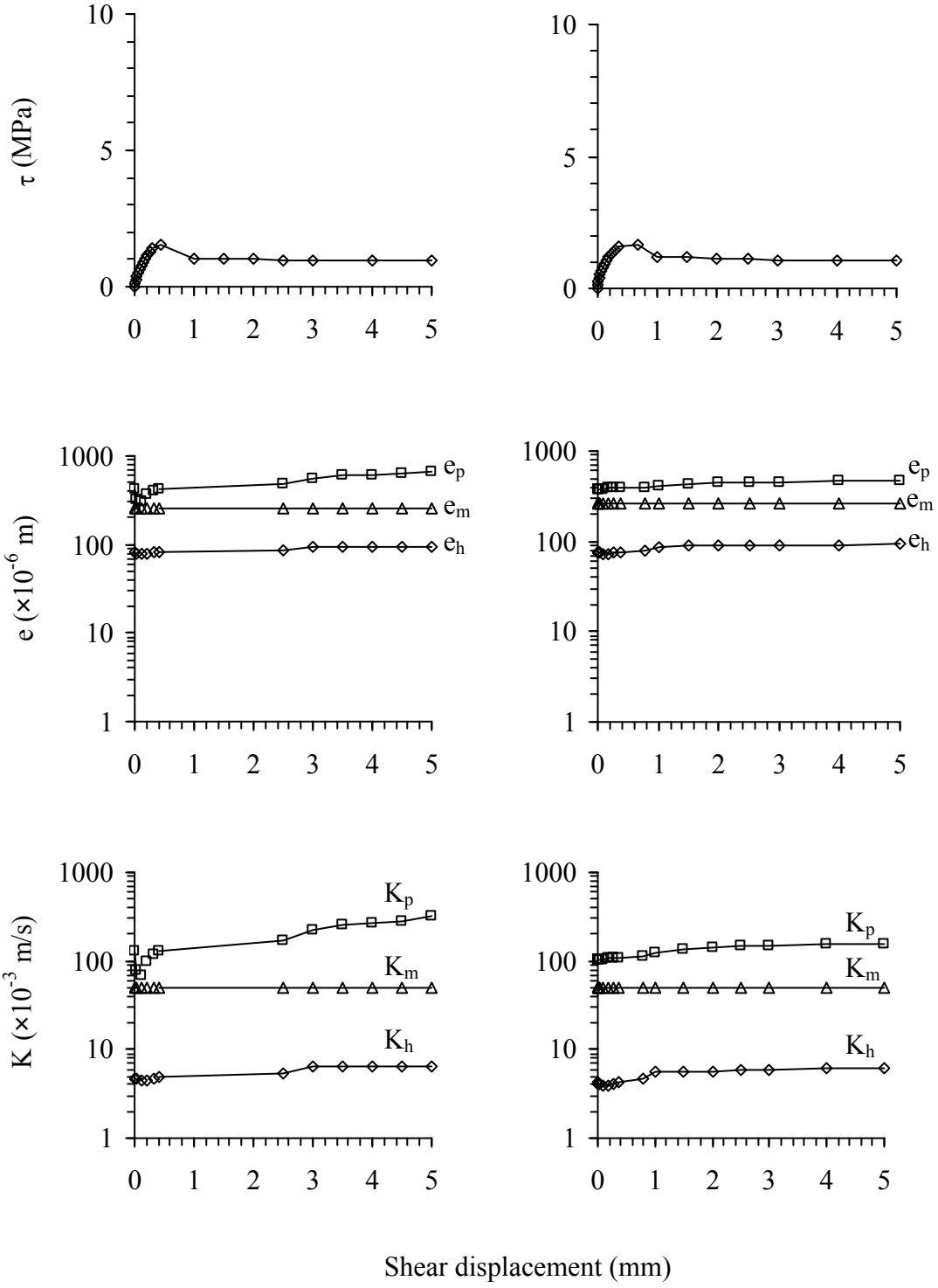

Figure 4.7(a) Shear stress, fracture aperture and hydraulic conductivity as a function of shear displacement (δ_s) at normal stress = 0.69 MPa (left) and 1.38 MPa (right) for SK sandstone.

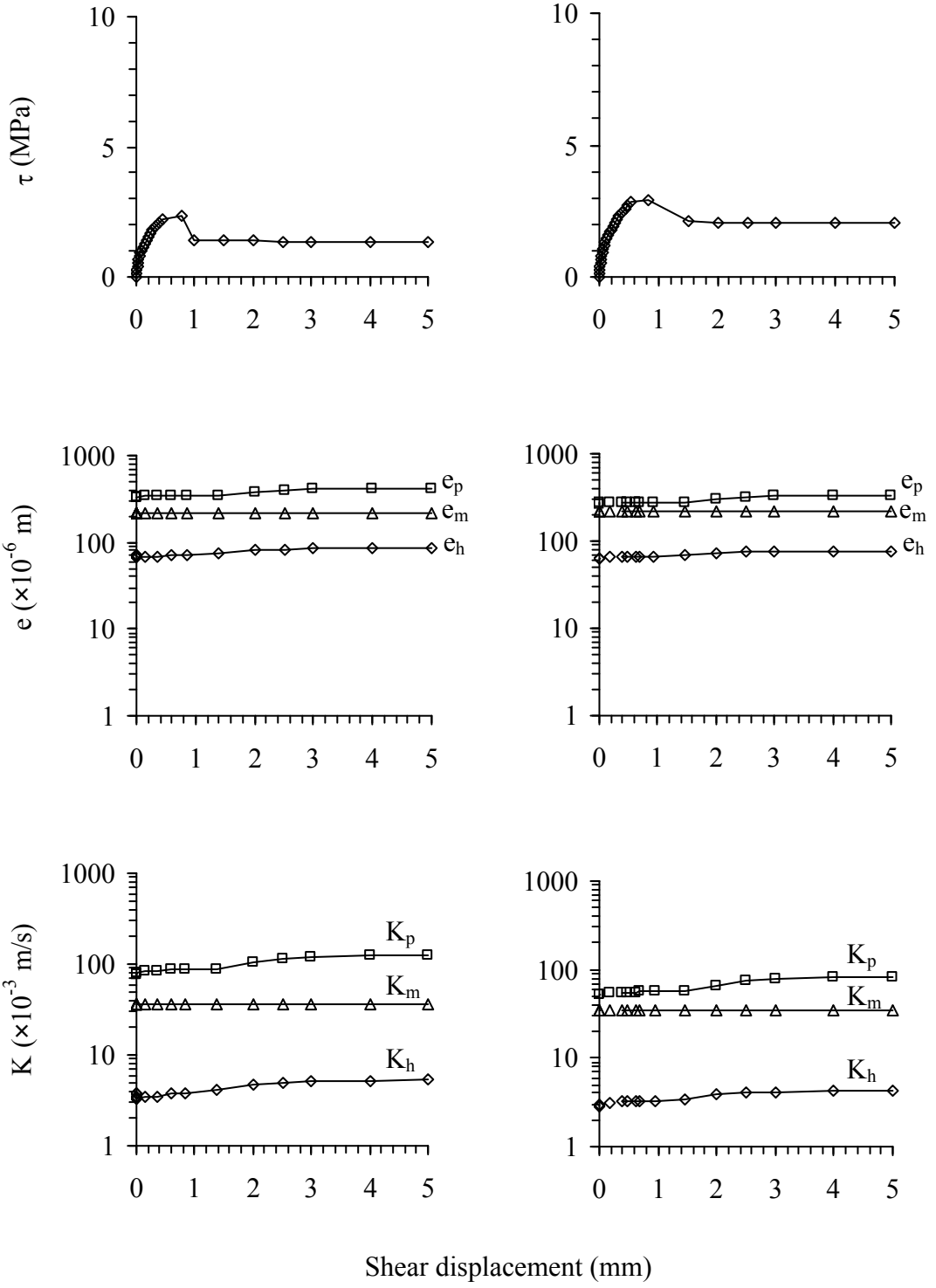

Figure 4.7(b) Shear stress, fracture aperture and hydraulic conductivity as a function of shear displacement (δ_s) at normal stress = 2.07 MPa (left) and 2.76 MPa (right) for SK sandstone.

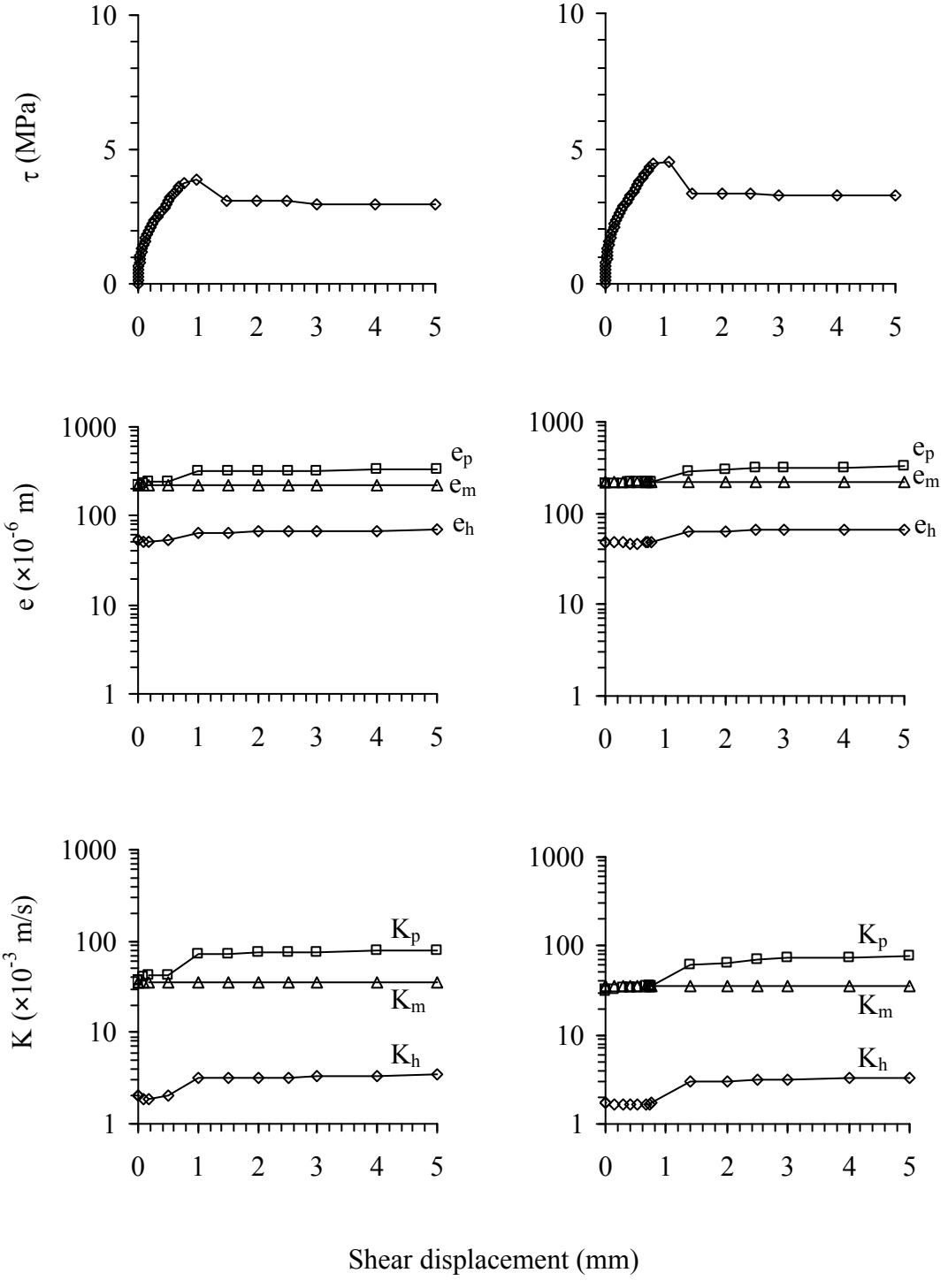

Figure 4.7(c) Shear stress, fracture aperture and hydraulic conductivity as a function of shear displacement (δ_s) at normal stress = 3.49 MPa (left) and 4.14 MPa (right) for SK sandstone.

Since the shear stresses after the peak value remain relatively consistent through 10 mm displacement, up to 3 mm shear displacement is plotted in the figures. Tables 4.2 through 4.5 show test parameters and results of the flow tests.

The fracture permeability is calculated from the equivalent hydraulic aperture (e_h) and from the physical aperture (e_p) for the peak ($K_{h,\ peak}$, $K_{p,\ peak}$) and residual ($K_{h,\ residual}$, $K_{p,\ residual}$) stresses.

For both peak and residual regions, the physical apertures are about 5 to 10 times greater than the hydraulic apertures, as a result the fracture hydraulic conductivity determined from the physical aperture are about one to two orders of magnitudes greater than these determined from the equivalent hydraulic apertures. This is probably became the measured physical apertures do not consider the effect of fracture roughness that causes a longer flow path.

Observations of pre– and post–test fracture areas suggest that no significant change has occurred in terms of fracture roughness. Even though some portion of fracture is sheared off, the JRC tends to remain the same. This is primarily because the applied normal stresses are relatively low. The mechanical aperture, e_m before, during and after shearing therefore remains constant for each fracture. As a result the hydraulic conductivity K_m calculated from e_m is independent of the shearing displacement. An example of the post–test fracture for PW sandstone is shown in Figure 4.8.

For PW, PP, PK and SK sandstones the physical aperture e_p tends to increase with shearing displacement. Its value fluctuates before the peak and tends to be more consistent in the residual stress region. The K_p values calculated from e_p subsequently show similar characteristics of the curves in the permeability-shear displacement diagram.

Table 4.2 Test parameters and results of PW sandstone.

Specimen No.	σ_n (MPa)	τ_{peak} (MPa)	$\tau_{residual}$ (MPa)	$e_{h,peak}$ ($\times10^{-6}$m)	$e_{h,residual}$ ($\times10^{-6}$m)	$e_{p,peak}$ ($\times10^{-6}$m)	$e_{p,residual}$ ($\times10^{-6}$m)	$K_{h,peak}$ ($\times10^{-3}$m/s)	$K_{h,residual}$ ($\times10^{-3}$m/s)	$K_{p,peak}$ ($\times10^{-3}$m/s)	$K_{p,residual}$ ($\times10^{-3}$m/s)
PW02	0.69	1.5	0.86	79	127.5	400	810	4.55	11.85	116.67	478.41
PW04	1.38	2.2	1.55	69.49	117.53	490	1030	3.52	10.07	175.07	773.57
PW03	2.07	2.97	2.28	62.36	110.49	420	1030	2.84	8.9	128.63	773.57
PW01	2.76	4.1	2.72	48.8	108.76	420	800	1.74	8.62	128.63	466.67
PW06	3.49	5.2	3.62	22.54	83.54	377	780	0.37	5.09	103.64	443.62
PW05	4.14	6.01	5.09	16.25	78.12	320.5	764.5	0.19	4.43	74.9	426.17

Table 4.3 Test parameters and results of PP sandstone.

Specimen No.	σ_n (MPa)	τ_{peak} (MPa)	$\tau_{residual}$ (MPa)	$e_{h,peak}$ ($\times10^{-6}$m)	$e_{h,residual}$ ($\times10^{-6}$m)	$e_{p,peak}$ ($\times10^{-6}$m)	$e_{p,residual}$ ($\times10^{-6}$m)	$K_{h,peak}$ ($\times10^{-3}$m/s)	$K_{h,residual}$ ($\times10^{-3}$m/s)	$K_{p,peak}$ ($\times10^{-3}$m/s)	$K_{p,residual}$ ($\times10^{-3}$m/s)
PP01	0.69	2.07	0.95	115.88	120.25	780	910	9.79	10.54	443.63	603.82
PP02	1.38	2.41	1.1	108.53	118.62	800	1110	8.59	10.26	466.67	898.41
PP06	2.07	2.97	1.47	80.56	102.18	386	860	4.73	7.61	108.64	539.29
PP04	2.76	4.07	2.37	44.27	96.83	337.5	447.5	1.43	6.84	83.06	146.02
PP05	3.49	5.47	3.28	17.88	90.66	255	420	0.23	5.99	47.41	128.63
PP03	4.14	5.99	3.79	22.54	89.94	250	415	0.37	5.9	45.57	125.58

Table 4.4 Test parameters and results of PK sandstone.

Sample No.	σ_n (MPa)	τ_{peak} (MPa)	$\tau_{residual}$ (MPa)	$e_{h,peak}$ ($\times10^{-6}$m)	$e_{h,residual}$ ($\times10^{-6}$m)	$e_{p,peak}$ ($\times10^{-6}$m)	$e_{p,residual}$ ($\times10^{-6}$m)	$K_{h,peak}$ ($\times10^{-3}$m/s)	$K_{h,residual}$ ($\times10^{-3}$m/s)	$K_{p,peak}$ ($\times10^{-3}$m/s)	$K_{p,residual}$ ($\times10^{-3}$m/s)
PK01	0.69	1.16	0.82	113.66	120.25	610	720	9.42	10.54	271.32	378
PK02	1.38	1.81	1.38	110.26	116.98	415	710	8.86	9.98	125.58	367.57
PK03	2.07	2.37	1.85	98.13	116.98	355	510	7.02	9.98	91.89	189.66
PK04	2.76	2.8	2.16	88.48	115.88	295	440	5.71	9.79	63.46	141.17
PK05	3.49	3.5	2.5	64.4	96.83	265	425	3.02	6.84	51.21	131.71
PK06	4.14	4.31	3.66	59.05	92.78	192.5	412.5	2.54	6.28	27.02	124.07

Table 4.5 Test parameters and results of SK sandstone.

Specimen No.	σ_n (MPa)	τ_{peak} (MPa)	$\tau_{residual}$ (MPa)	$e_{h,peak}$ ($\times10^{-6}$m)	$e_{h,residual}$ ($\times10^{-6}$m)	$e_{p,peak}$ ($\times10^{-6}$m)	$e_{p,residual}$ ($\times10^{-6}$m)	$K_{h,peak}$ ($\times10^{-3}$m/s)	$K_{h,residual}$ ($\times10^{-3}$m/s)	$K_{p,peak}$ ($\times10^{-3}$m/s)	$K_{p,residual}$ ($\times10^{-3}$m/s)
SK01	0.69	1.55	1.03	85.44	94.15	485	550	5.32	6.46	171.52	220.57
SK02	1.38	1.64	1.12	80.56	89.94	390	450	4.73	5.9	110.91	147.66
SK03	2.07	2.37	1.38	75.17	82.23	350	400	4.12	4.93	89.32	116.67
SK04	2.76	2.93	2.07	69.05	75.17	280	330	3.48	4.12	57.17	79.41
SK05	3.49	3.88	3.1	52.64	65.62	240	315	2.02	3.14	42	72.35
SK06	4.14	4.53	3.32	48.8	65.62	220	310	1.74	3.14	35.29	70.07

The hydraulic aperture e_h indirectly determined from the inflow rates also tends to increase with the shear displacement, particularly under high normal stresses. Even though K_p and K_h show similar characteristics of the curves in the permeability-shear displacement diagram, K_p is always about an order of magnitude greater than K_h, particularly in the residual shear region.

4.4 Effect of normal stresses

Figures 4.9 plotted the hydraulic conductivity derived from e_h as a function of normal stress σ_n. The fracture permeability values under no shear stress, immediately before the peak stress, and under the residual shear stress are compared. The fracture permeability under residual shear region is greater than that under no shear and that immediately before peak stress. It is not very sensitive to the normal stress – showing

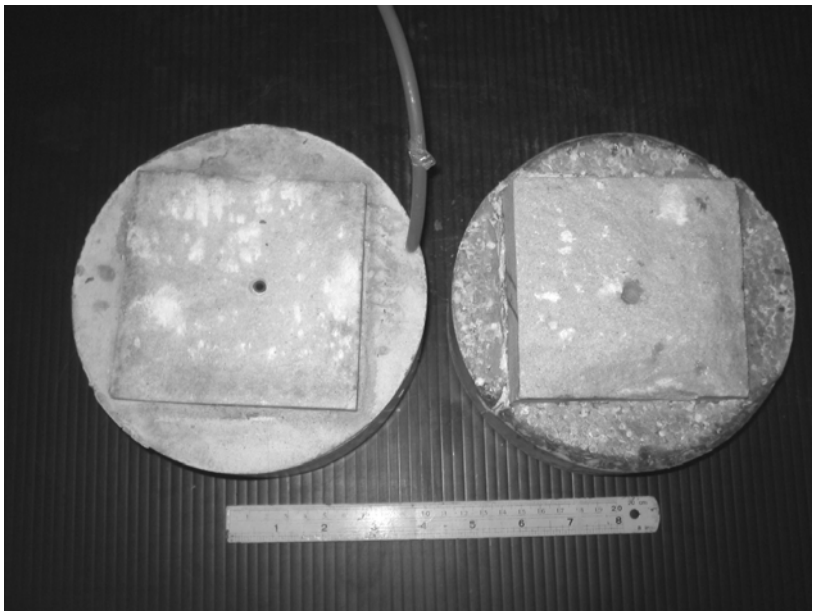

Figure 4.8 Example of post-test fracture surfaces in a PW sandstone specimen. The sheared surfaces are indicated by white areas.

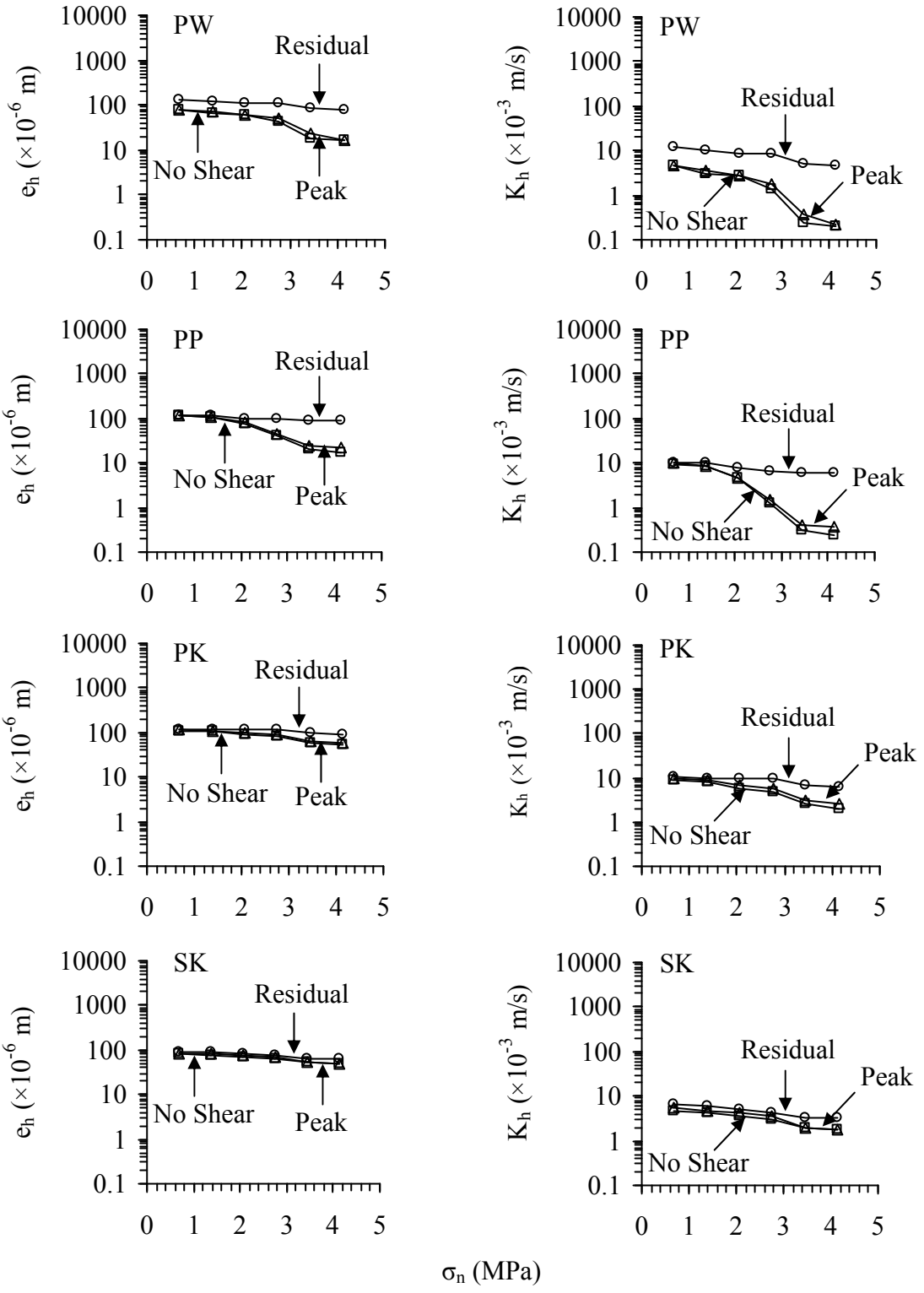

Figure 4.9 Hydraulic aperture (e_h) and hydraulic conductivity (determined from e_h) as a function of normal stress (σ_n) for PW, PP, PK and SK sandstones.

a slightly decrease with increasing the normal stress. The magnitudes of fracture permeability under no shear and under peak stress are similar. Both tend to decrease exponentially with the normal stress. As a result the difference between the permeability under residual shear stress and that under peak stress becomes larger as the normal stress increases. The results agree reasonably well with those obtained by Lee and Cho (2002) and Son et al. (2004).

This suggests that under a given normal stress, the fracture permeability immediately before peak stress will remain similar to that under no shear stress. After the fracture is displaced beyond the peak stress, its permeability however notably increases particularly under high normal stresses. Figure 4.10 plots the shear stress as a function of normal stress filled with the Coulomb criterion. The shear strength of the four sandstones is comparable.

4.5 Effect of shear strength on fracture

The fracture hydraulic conductivity decreases with increasing fracture shear strength. Figures 4.11 through 4.14 plots the fracture hydraulic conductivity (K_h) as a function of fractures shear strength. The decrease of the K_h with the peak shear strength can be represented by an exponential equation:

$$K_h = \alpha_p \exp(\beta_p \tau_p) \tag{4.6}$$

where α_p and β_p are empirical constants.

For the residual shear strength the change of K_h can be represented by

$$K_h = \alpha_r \exp(\beta_r \tau_r) \tag{4.7}$$

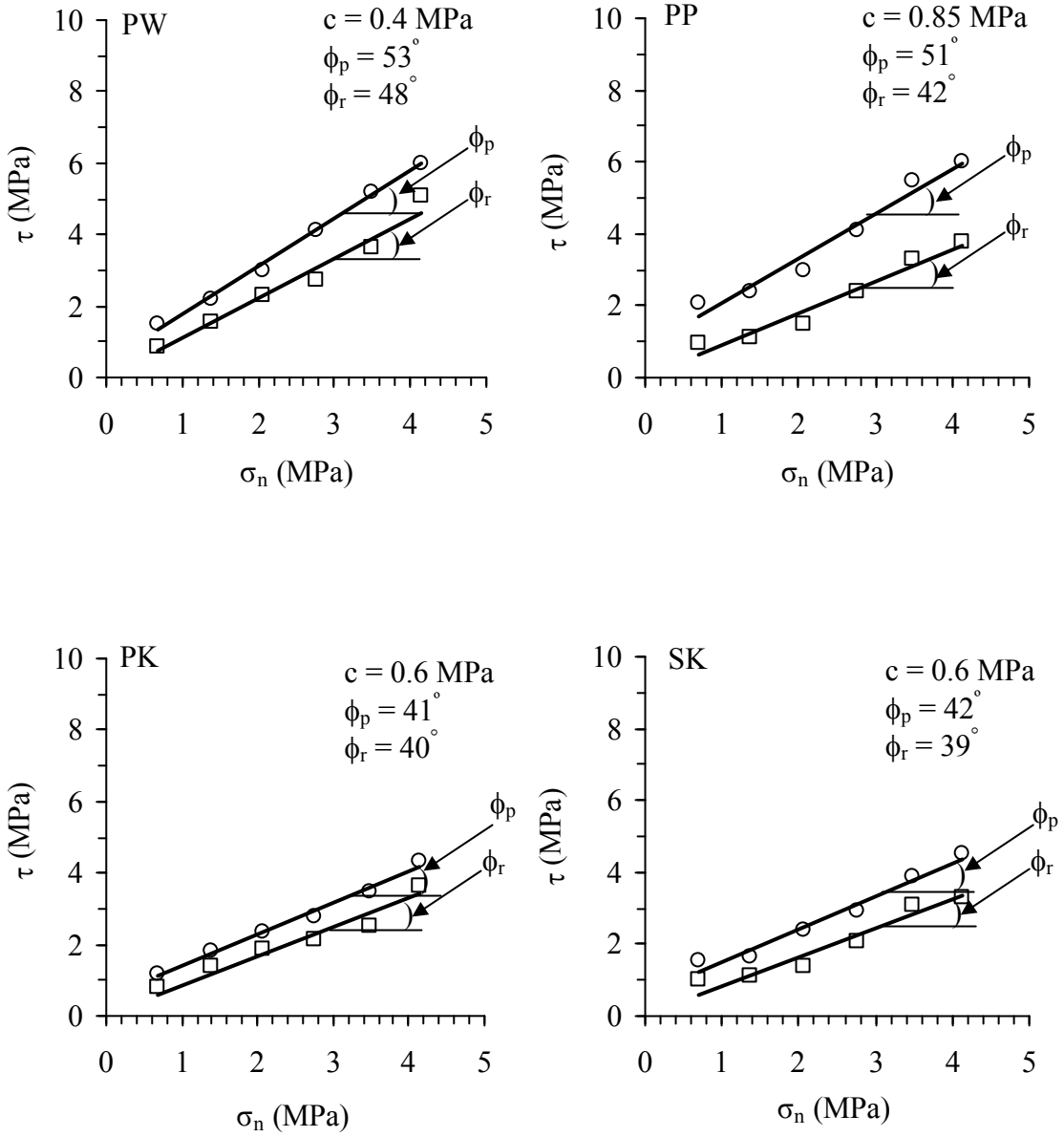

Figure 4.10 Shear stress as a function of normal stress and filled with the coulomb criterion.

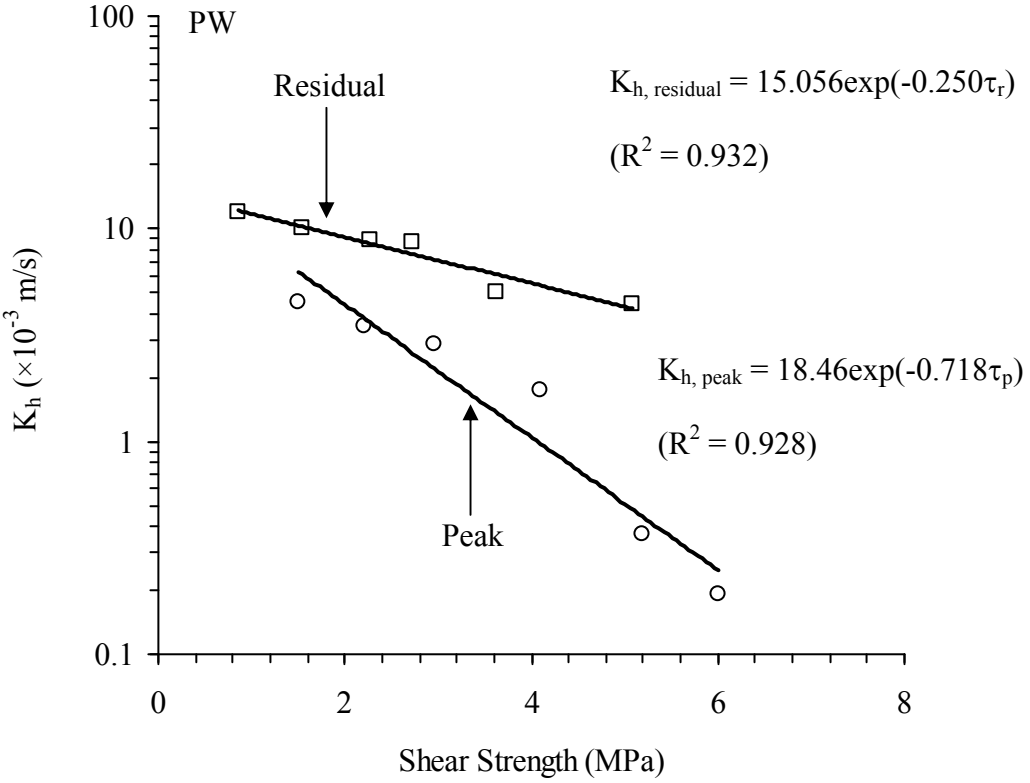

Figure 4.11 Hydraulic conductivity (K_h) as a function of peak and residual shear strength for PW sandstone.

where α_r and β_r are empirical constants.

The exponent β_p and β_r represent the reduction rate of the fracture permeability as the fracture shear strength increases. The hydraulic conductivity determined under peak strength tends to decrease more rapid than that determined under residual strength. Assuming that the Coulomb criterion is valid for these sandstone fractures, the above relations can be used to estimates the fracture permeability with shear strength higher than the range tested here.

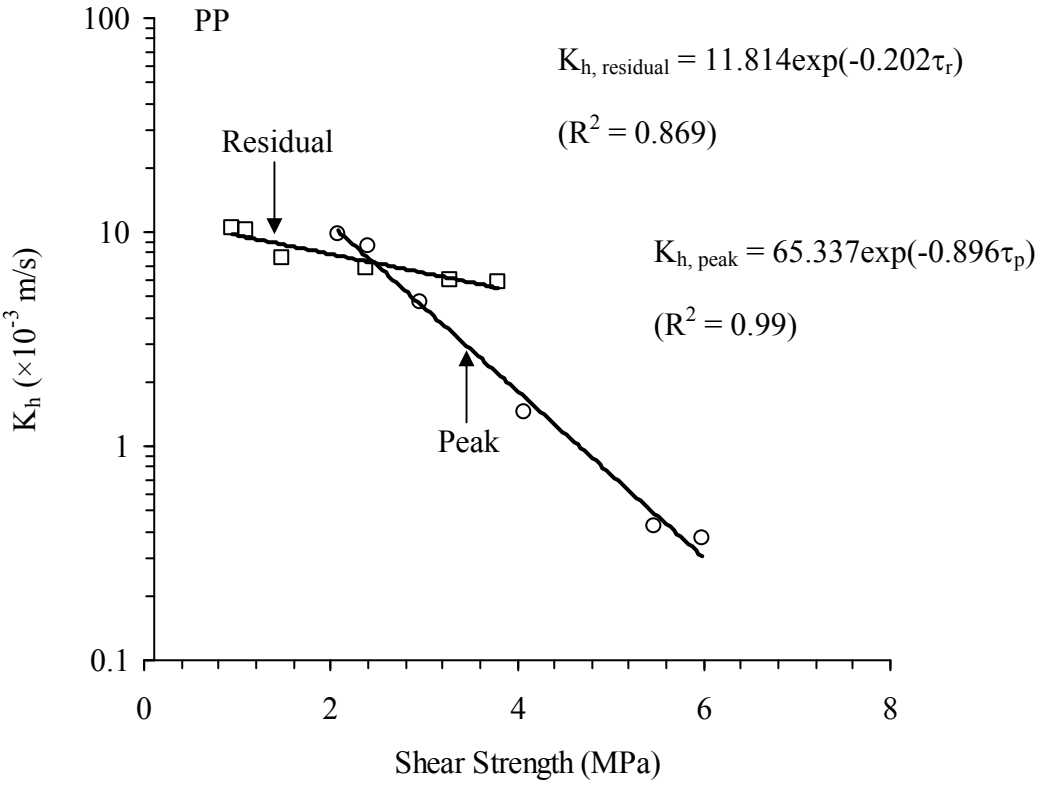

Figure 4.12 Hydraulic conductivity (K_h) as a function of peak and residual shear strength for PP sandstone.

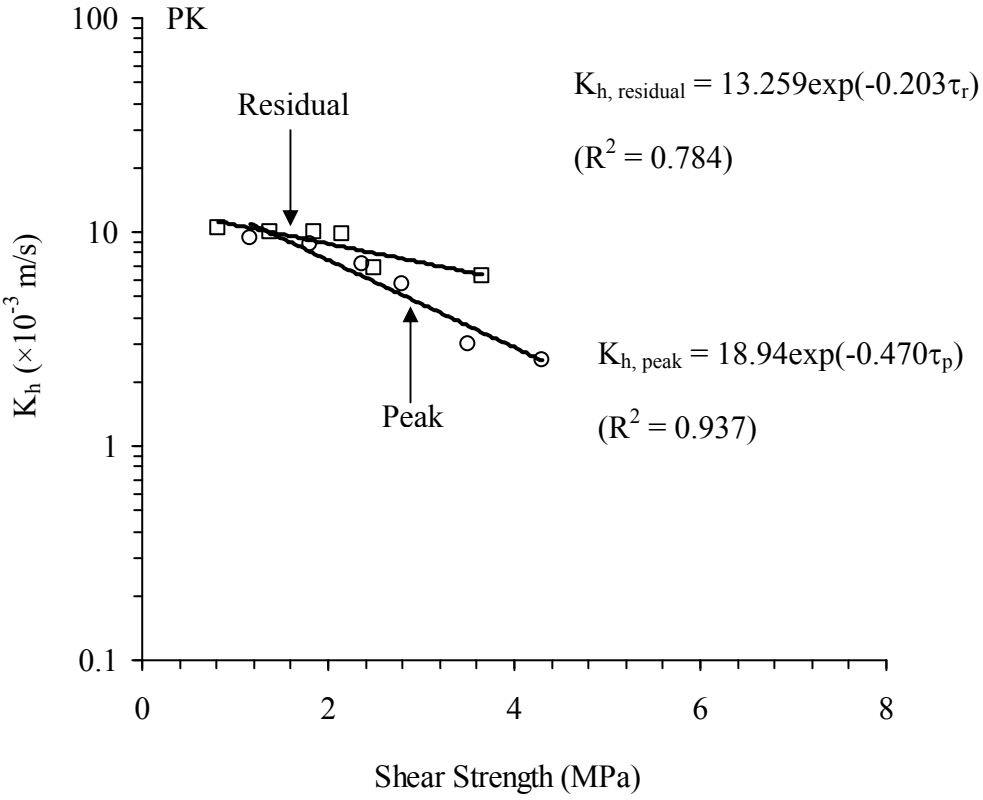

Figure 4.13 Hydraulic conductivity (K_h) as a function of peak and residual shear strength for PK sandstone.

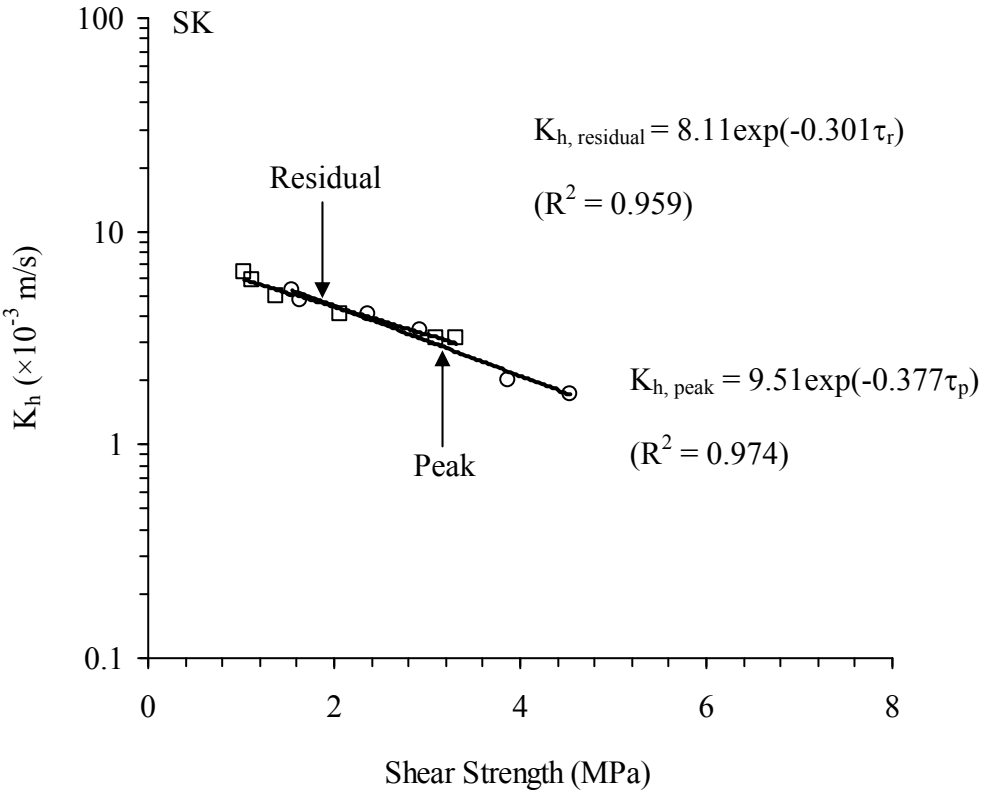

Figure 4.14 Hydraulic conductivity (K_h) as a function of peak and residual shear strength for SK sandstone.

CHAPTER V

DISCUSSIONS AND CONCLUSIONS

5.1 Discussions and conclusions

Falling head flow tests have been performed to determine the fracture permeability of tension-induced fractures under normal and shear stresses. The changes of the physical and hydraulic apertures, the water flow rates, and the applied shear stresses has been monitored and used to calculate the changes of the fracture permeability as a function of shear displacement. The results indicate that the physical aperture e_p and hydraulic aperture e_h increase with shearing displacement, particularly under high normal stresses. The magnitudes of fracture permeability under no shear and under peak shear stress are similar. For both peak and residual regions, the physical apertures are about 5 to 10 times greater than the hydraulic apertures, as a result the fracture hydraulic conductivity determined from the physical aperture are about one to two orders of magnitudes greater than these determined from the equivalent hydraulic apertures. This is probably because the measured physical apertures do not consider the effect of fracture roughness that causes a longer flow path.

In the residual strength region the fracture permeability is not sensitive to the normal stress – showing a slightly decrease with increasing the normal stress. The magnitudes of fracture permeability under no shear and under peak stress are similar. Both tend to decrease exponentially with the normal stress. As a result the difference

between the permeability under residual shear stress and that under peak stress becomes larger as the normal stress increases.

This suggests that under a given normal stress, the fracture permeability immediately before peak stress will remain similar to that under no shear stress. After the fracture is displaced beyond the peak stress, its permeability however notably increases particularly under high normal stresses.

The difference between the permeability under residual shear stress and that under peak stress becomes larger under higher normal stresses. The fracture hydraulic conductivities exponentially decrease with increasing the normal stresses. Their permeability is in the range between 0.1×10^{-3} m/s and 10×10^{-3} m/s. The fracture hydraulic conductivity determined here compares well with those obtained by Zhao (1998) and Chandra et al. (2008).

The flow in fractures is sensitive to normal stiffness of discontinuity. The normal stiffness will increase with increasing stress. In this research, the range of normal stiffness is approximately from 1 to 10 GPa/m which is of the same order of magnitude with those obtained by Pyrak-Nolte et al. (2000).

5.2 Recommendations for future studies

The test results for the four sandstones are well coincided. This is probably because these sandstones have similar strength and texture. To confirm the conclusions drawn in this research, more testing is required as follows.

1. Similar test should be performed on rock with higher strength and larger grain size and under a variety of JRC values.

2. A relationship between the fracture roughness and fracture permeability before and after the peak shear strength should be determined.

3. The fracture permeability should be obtained from shearing specimen while the dilation is maintained constant.

4. The hydraulic head should be applied at different levels and using gas as flow medium.

REFFERENCES

ASTM D5607-95, Standard test method for performing laboratory direct shear strength test of rock specimens under constant normal force. Annual Book of ASTM Standards, 04.08, **American Society for Testing and Materials**, Philadelphia.

Auradou, A., Drazer, G., Boschan, A., Hulin, J.P., and Koplik, J. (2006). Flow channeling in a single fracture induced by shear displacement. **Geothermics**. 35(5-6): 576–588.

Baghbanan, A. and Jing, L. (2006). Hydraulic properties of fractured rock masses with correlated fracture length and aperture. **International Journal of Rock Mechanics and Mining Sciences**. 44 (5): 704–719.

Baghbanan, A. and Jing, L. (2008). Stress effects on permeability in a fractured rock mass with correlated fracture length and aperture. **International Journal of Rock Mechanics and Mining Sciences**. 45(8): 1320-1334.

Bandis, S.C., Barton, N.R., and Christianson, M. (1985). Application of a new numerical model of joint behavior to rock mechanics problems. In **Proceeding of the International Symposium on Fundamentals of Rock Joints**. 24(4): 132

Bandis, S.C., Lumsden, A.C., and Barton, N.R. (1983). Fundamentals of rock Joint deformation. **International Journal of Rock Mechanics and Mining Sciences**. 20(6): 249-268.

Barton, N. (1973). Review of a new shear-strength criterion for rock joints. **Engineering Geology**. 7(4): 287-332.

Barton, N., Bandis, S., and Bakhtar, K. (1985). Strength, Deformation and conductivity coupling of rock joints. **International Journal of Rock Mechanics and Mining Sciences**. 22(3): 121-140.

Brown, E.T. (editor) (1981). Rock Characterization testing and monitoring: ISRM Suggested methods. The Commission on Rock Testing Methods, **International Society for Rock Mechanics**. 211 pp.

Chandra, S., Ahmed, S., Ram, A., and Dewandel, B. (2008). Estimation of hard rock aquifers hydraulic conductivity from geoelectrical measurements : A theoretical development with field application. **Journal of Hydrology**. 357(3-4): 218-227.

Ferfera, F.M.R., Sarda, J-P., Bouteca, M. and Vincke, O. (1997). Experimental study of monophasic permeability changes under various stress paths. **International Journal of Rock Mechanics and Mining Sciences**. 34(3-4): 3-4.

Fleuter, W.F. (1997). Analytical and experimental investigation into the shear performance of joints in soft sedimentary rocks. **MEngSc dissertation. Australia** : Department of Civil Engineering, Monash University.

Freeze, R.A. and Cherry, J.A. (1979). **Groundwater**. Prentice Hall, Englewood Cliffs.

Giacominia, A., Buzzib, O., Ferreroa, A.M., Migliazzaa, M., and Giania, G.P. (2008). Numerical study of flow anisotropy within a single natural rock joint. **International Journal of Rock Mechanics and Mining Sciences**. 45 (1): 47–58.

Hamiel, Y., Lyakhovsky, V., and Agnon, A. (2005). Rock dilation, nonlinear deformation, and pore pressure change under shear. **A Institute of Earth Sciences**, Hebrew University of Jerusalem.

Hans, J. (2002). Etude expérimentale et modélisation numérique multiéchelle du comportement hydromécanique des répliques de joints rocheux. **PhD thesis, Joseph Fourier University**, Grenoble, France, 2002.

Indraratna, B. and Ranjith, P.G. (2001). Laboratory measurement of two-phase flow parameters in rock joints based on high pressure triaxial testing. **Journal of Geotechnical and Geoenvironmental Engineering**. 127(6): 530-542.

Indraratna, B. and Ranjith, P. (2001). Hydromechanical Aspects and Unsaturated Flow in Joints Rock. **Lisse : A. A. Balkema**.

Jiang, X.W., Wan, L., Wang, X.S., Liang, S.H., and Hu, B.X. (2009). Estiimation of fracture normal stiffness using a transmissivity-depth correlation. **International of Rock Mechanics and Mining Sciences**. 46(1): 51-58.

Jiang, Y., Tanabashi, Y., Xiao, J., and Nagaie (2004). An improved shear-flow test apparatus and its application to deep underground construction. Paper 1A 28 — SINOROCK2004 Symposium. **Internationa Journal of Rock Mechanics and Mining Sciences**. Vol. 41, No. 3, CD-ROM.

Lee, H.S. and Cho, T.F. (2002). Hydraulic characteristics of rough fractures in linear flow under normal and shear load. **Rock Mechanics and Rock Engineering**, Springer-Verlag Wien. 35(4): 299-318.

Lee, S.D. and Harrison, J.P. (2001). Empirical parameters for non-linear fracture stiffness from numerical experiments of fracture closure. **International of Rock Mechanics and Mining Sciences**. 38(5): 721-727.

Maini, Y.N.T. (1971). In situ hydraulic parameters in jointed rock-their measurement and interpretation. **Ph.D. Thesis. Imperial College, London**. 321 p.

Niemi, A.P., Vaittinen, T.A., Vuopio, J.A., and Polla, J.P. (1997). Simulation of heterogeneous flow in a natural fracture under varying normal stress. **International of Rock Mechanics and Mining Sciences**. 34(3-4): 565.

Oda, M., Takemura, T., and Aoki, T. (2002). Damage growth and permeability change in triaxial compression tests of Inada granite. **Mechanics of Materials**. 34(6): 313–331.

Pearce, H. A micro-mechanical approach to the shear behavior of rock joints. **Ph.D. dissertation. Australia** : Department of Civil Engineering, Monash University.

Pusch, G. and Weber, J.R. (1998). Correlation of rock permeability and anisotropic stress conditions for the integration of rock mechanical and hydraulic flow models. **SCA Paper 9826**.

Pyrak-Noltea, L.J. and Morrisa, J.P. (2000). Single fractures under normal stress: The relation between fracture specific stiffness and fluid flow. **International Journal of Rock Mechanics and Mining Sciences**. 37(1): 245-262.

Seidel, J.P. and Haberfield, C.M. (2002). A theoretical model for rock joints subjected to constant normal stiffness direct shear. **International of Rock Mechanics and Mining Sciences**. 39(5): 539-553.

Shangxian, Y. and Shangxu W. (2006). Effect and mechanism of stresses on rock permeability at different scales. **Science in China: Series D Earth Sciences 2006**. 49(7): 714-723.

Son, B.K., Lee, Y.K., and Lee, C.I. (2004). Elasto-plastic simulation of a direct shear test on rough rock joints. **International Journal of Rock Mechanics and Mining Sciences**. 41(3): 1-6.

Xiao, Y.X., Lee, C.F., and Wang, S.J. (1999). Assessment of an equivalent porous medium for coupled stress and fluid flow in fractured rock. **International Journal of Rock Mechanics and Mining Sciences**. 36(7): 871-881.

Zangerl, C., Evans, K.F., Eberhardt, E., and Loew, S. (2008). Normal stiffness of fractures in granitic rock : A compilation of laboratory and in-situ experiments. **International Journal of Rock Mechanics and Mining Sciences**. 45(8): 1500-1507.

Zeigler, B. 1976. **Theory of Modelling and Simulation**. New York: John Wiley and Sons.

Zhao, J. (1998). Rock mass hydraulic conductivity of the Bukit Timah granite, Singapore. **Engineering Geology**. 50(1-2): 211-216.

Zhou, J.J. and Shao, J.F. (2006). Micromechanical study of damage growth and permeability variation in brittle rocks. **Studia Geotechnica et Mechanica**. Vol. 28, No. 1, 2006.

Zhu, W., Montési, L.G.J. and Wong, T.F. (2002). Effects of stress on the anisotropic development of permeability during mechanical compaction of porous sandstones. **Geological Society, London, Special Publications**; 2002; v. 200; p. 119-136.

APPENDIX A

SHEAR STRESS-DISPLACEMENT CURVES

FROM DIRECT SHEAR TESTS

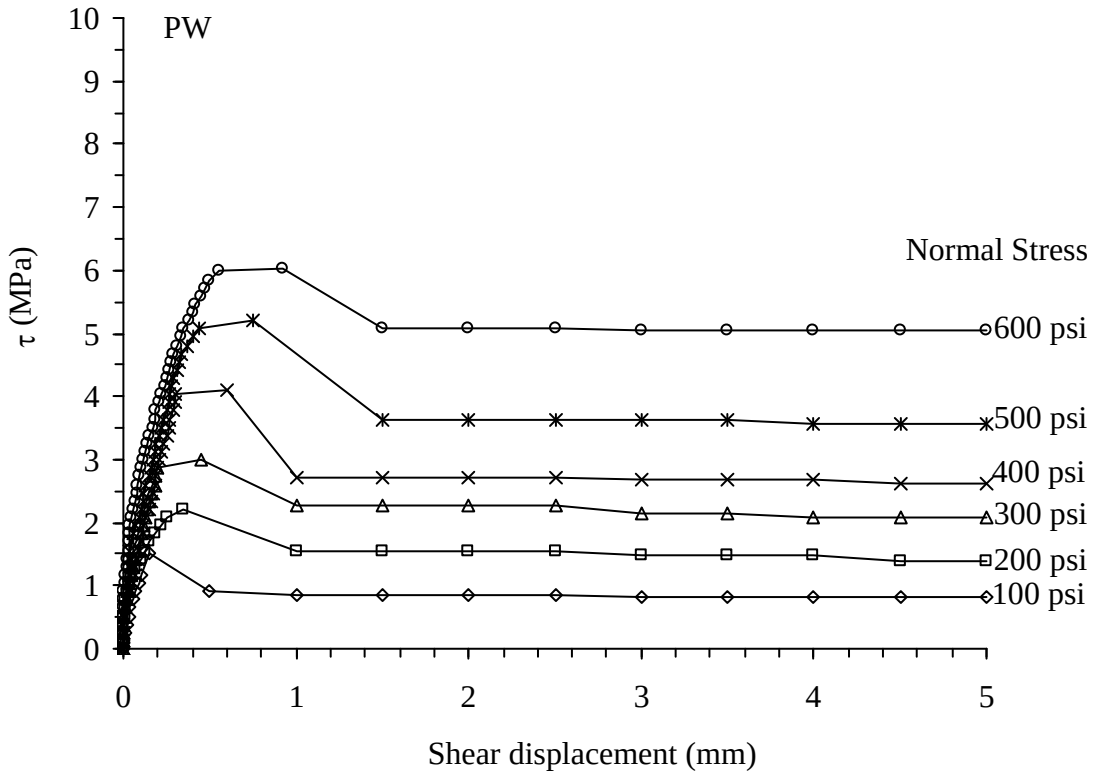

Figure A.1 Shear stress as a function of shear displacement for PW sandstones.

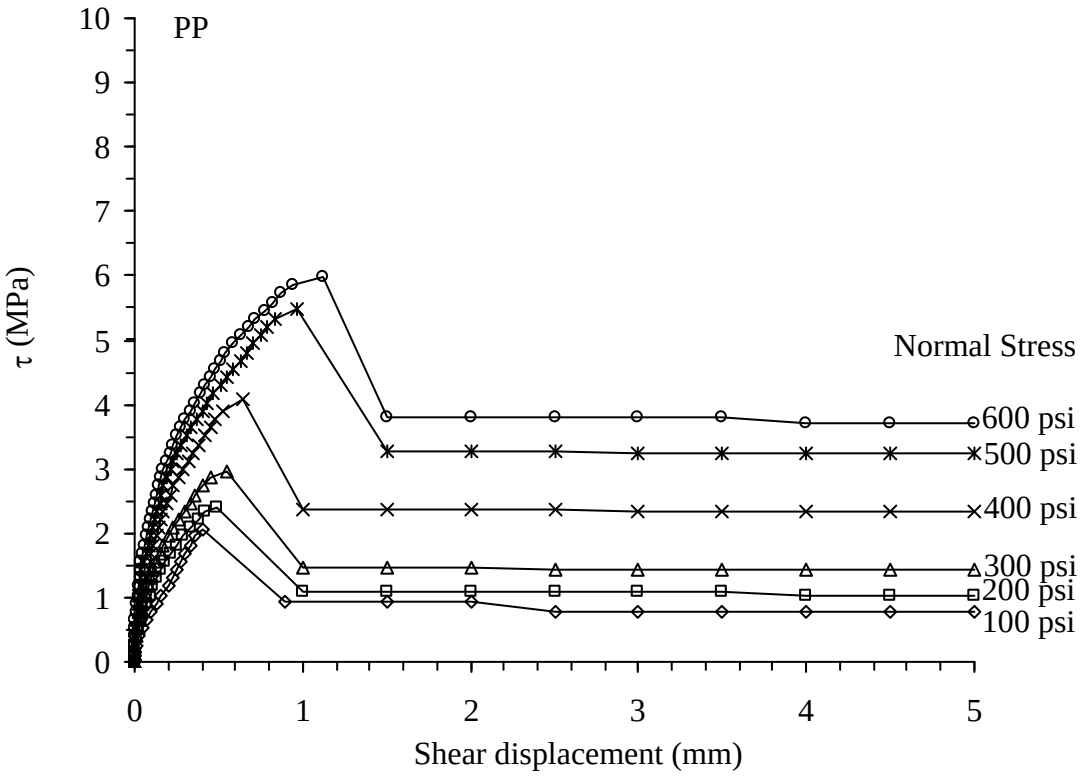

Figure A.2 Shear stress as a function of shear displacement for PP sandstones.

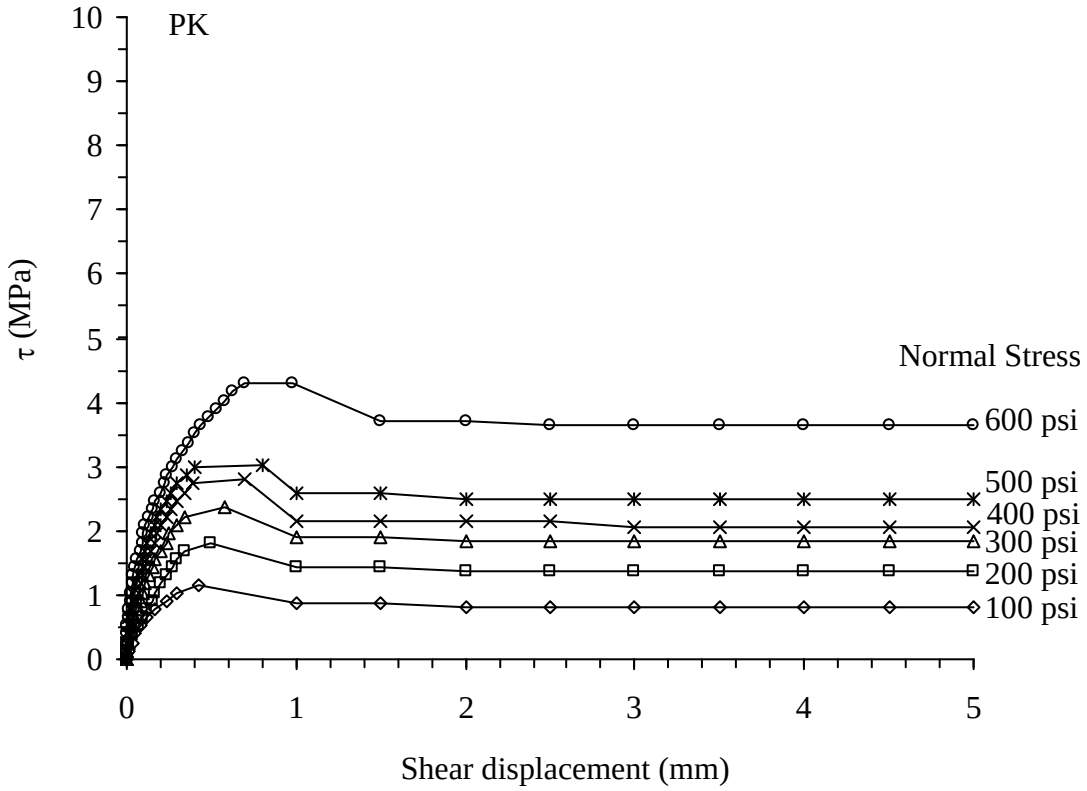

Figure A.3 Shear stress as a function of shear displacement for PK sandstones.

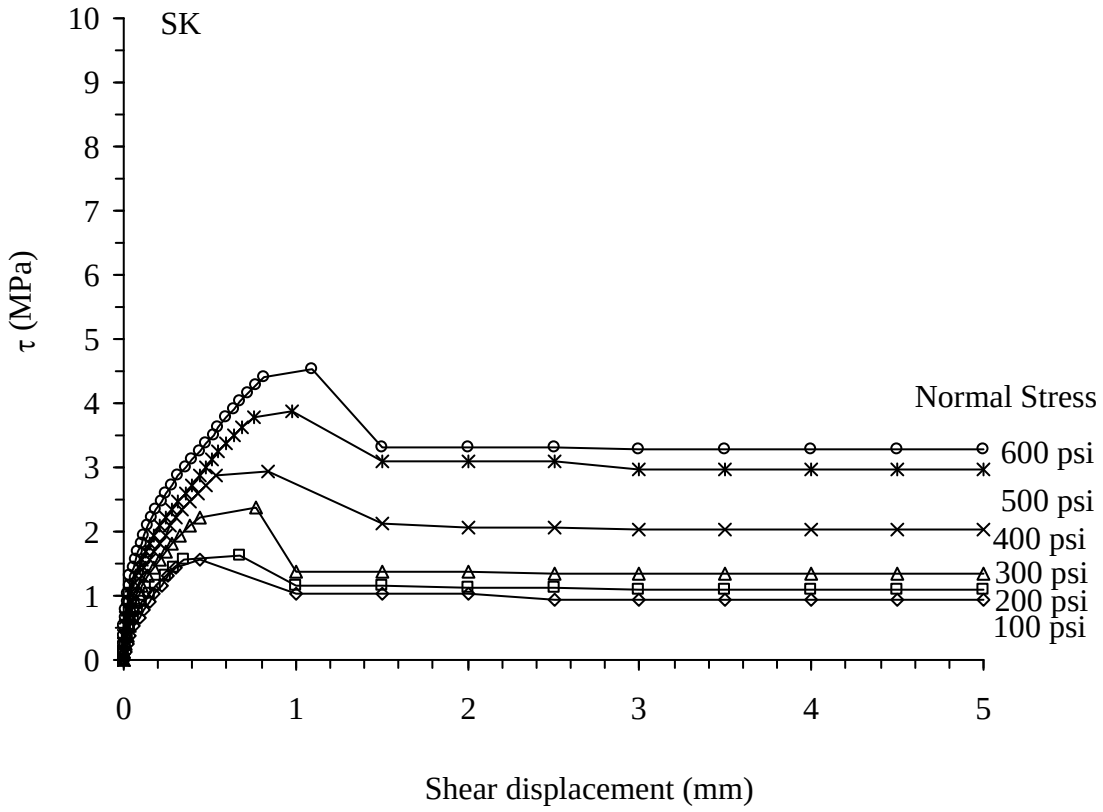

Figure A.4 Shear stress as a function of shear displacement for SK sandstones.

APPENDIX B

TECHNICAL PUBLICATION

TECHNICAL PUBLICATION

Akkrachattrarat, N., Suanprom, P., Buaboocha, J. and Fuenkajorn, K., 2009. **Flow testing of sandstone fractures under normal and shear shear stresses**, In Proceedings of the Second Thailand Symposium on Rock Mechanics (ThaiRock 2009), Jomtien Palm Beach Hotel & Resort, Chonburi, 12-13 March 2009, pp. 319 – 334.

Rock Mechanics, Fuenkajorn & Phien-wej (eds) © 2009. ISBN 978 974 533 624 7

Flow testing of sandstone fractures under normal and shear stresses

N. Akkrachattrarat, P. Suanprom, J. Buaboocha & K. Fuenkajorn
Geomechanics Research Unit, Suranaree University of Technology, Thailand

Keywords: Permeability, fracture, aperture, shear stress, deviatoric stress

ABSTRACTS: Flow tests have been performed to determine hydraulic conductivity of intact sandstone specimens under confining pressures and deviatoric stresses, and of tension-induced fractures under normal and shear stresses. The results indicate that the intact sandstone permeability decreases with increasing volumetric strain before dilation strength probably due to the closure of voids and micro-cracks, and increases with the specimen dilation after the dilation strength probably due to the initiation and propagation of cracks and fractures. The physical aperture e_p and hydraulic aperture e_h increase with shearing displacement, particularly under high normal stresses. The magnitudes of fracture permeability under no shear and under peak shear stress are similar. The K_p is about an order of magnitude greater than K_b, particularly in the residual shear region. Both tend to decrease exponentially with increasing normal stress. The difference between the permeability under residual shear stress and that under peak stress becomes larger under higher normal stresses. The fracture hydraulic conductivities exponentially decrease from 10000×10^{-6} m/s to 100×10^{-6} m/s as the normal stresses are increased from 0.35 MPa to 2.06 MPa. Under normal stress alone a permanent fracture closure is usually observed after unloading as evidenced by the permanent reduction of the measured flow rates.

1 INTRODUCTION

Groundwater in rock mass is one of the key factors governing the mechanical stability of slope embankments, underground mines and tunnels. The lack of proper understanding of the water pressure and flow characteristics in rock mass makes it difficult to predict the water inflow for underground mines and tunnels under complex hydro-geological environments. Unlike those in the soil mass, permeability of rock mass is path dependent, controlling mainly by the system of fracture as the permeability of the intact rocks is normally low. For undisturbed rock mass (before excavation) the joint characteristics (e.g., roughness, aperture, spacing and orientation) that dictate the amount and direction of water flow, can be adequately determined by means of in-situ measurements, and are sometimes assisted by numerical modeling. Slope or underground excavations disturb the surrounding rock, alter the stress states on the fracture planes, and often cause relative displacements of the rock fractures. In most cases the excavations usually increase the surrounding rock mass permeability, sometimes by several orders of magnitude.

It has been experimentally found that permeability of intact rocks is affected by the confining pressures (Iscan et al., 2006; Shangxian & Shangxu, 2006) and by deviatoric stresses (Ferfera et al., 1997; Oda, 2002; Pusch & Weber, 1998; Heiland, 2003; Zhou & Shao, 2006). The rock permeability generally decreases logarithmically with increasing the confining pressures. Under deviatoric stresses the rock permeability first decreases due to a reduction of pore spaces, and starts to increase due to the damage growth after the rock is dilated under differential stresses.

Fracture apertures and hydraulic conductivity are the main factors governing the rock mass permeability. Xiao et al. (1999), Pyrak-Noltea & Morrisa (2000), Niemi et al. (1997), Indraratna & Ranjith (2001) and Baghbanan & Jing (2008) conclude from their experimental results that fracture permeability exponentially decreases with increasing normal stresses. The apertures and permeability of rock fractures are also affected by the shearing displacement (Auradou et al., 2006). The flow testing results on fractures in granite and marble by Lee & Cho (2002) indicate that the fracture permeability increases by up to two orders of magnitude as the shearing displacement increases. This finding is supported by the results of numerical simulations by Son et al. (2004).

The objective of this study is to experimentally determine the hydraulic conductivity of fractures in sandstone specimens under normal and shear stresses. Constant head flow tests are conducted to obtain data basis on the permeability of intact sandstones under hydrostatic pressures and deviatoric stresses. The rock permeability is correlated with the volumetric strain before failure and with the volumetric dilation after failure. Falling head tests are performed to determine the permeability of tension-induced fractures under normal and shear stresses. The flow rates are monitored from before peak shear strength through residual shear strength. The fracture hydraulic conductivities calculated from the physical, mechanical and hydraulic apertures are compared. The joint normal and shear stiffness parameters are determined.

2 ROCK SAMPLES

The tested sandstones are from four sources: Phu Phan, Phra Wihan, Phu Kradung and Sao Kua formations (hereafter designated as PP, PW, PK and SK sandstones). They belong to the Khorat group and widely expose in the north and northeast of Thailand. X-ray diffraction analyses have been performed to determine their mineral compositions. Table 1 summarizes the results. These fine-grained quartz sandstones are selected for this study primarily because they have highly uniform texture, grain size and density.

3 FLOW TESTING ON INTACT SANDSTONES

3.1 Permeability of Intact Sandstones under Confining Pressures

Constant head flow tests have been performed to assess the effects of hydrostatic pressures and deviatoric stresses on the intact sandstone permeability. Figure 1 shows the laboratory arrangement of the constant head flow test under various confining pressures. The sandstone specimens have a nominal dimension of 5 cm in diameter and 10 cm long. A constant diameter water pump is used to inject water pressure of 0.14 MPa (20 psi) to bottom end of the specimen while the specimen is confined in a triaxial cell. The injected water pressure is controlled by using a regulating valve at the top of nitrogen gas tank. The constant confining pressures vary from 3.45 (500 psi), 6.90, 10.34, 13.79, 17.24 to 20.69 MPa (3000 psi). A

Rock Mechanics, Fuenkajorn & Phien-wej (eds) © 2009. ISBN 978 974 533 624 7

Table 1. Mineral compositions of tested sandstones obtained from X-ray diffraction.

Rocks	Density (g/cc)	Grain Size (mm)	Sorting	Mineral Compositions				
				Quartz (%)	Albite (%)	Kaolinite (%)	Feldspar (%)	Mica (%)
PW	2.35	1.5-2.0	well	99.47	-	0.53	-	-
PP	2.45	1.5-2.0	well	98.40	-	-	-	1.60
PK	2.63	0.1-1.5	moderate	48.80	46.10	5.10	-	-
SK	2.37	0.1-1.0	poorly	57.00	39.50	-	2.90	0.60

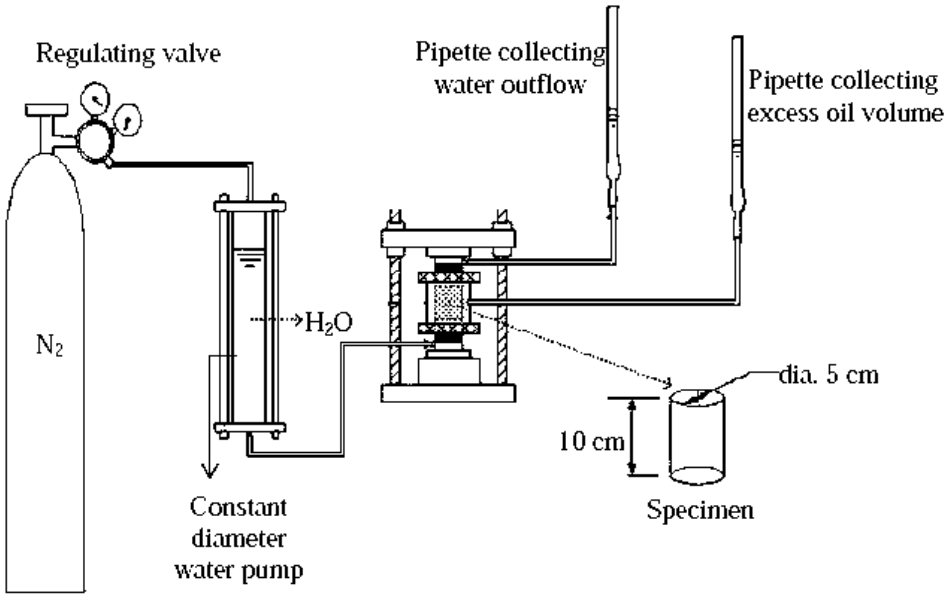

Figure 1. Laboratory arrangement for constant head flow tests.

high precision pipette collects the outflow of water at the top end of the specimen. The measured flow rates under each confining pressure are used to calculate the specimen permeability. The hydraulic conductivity (K) is calculated by assuming that the Darcy's law is valid (Indraratna & Ranjith, 2001):

$$K = 4q\mu / [\pi D^2(dp/dx)] \quad (1)$$

where q is water flow rate through the specimen (cm^2/s), μ is the dynamic viscosity of the water ($N{\cdot}s/cm^2$), D is the specimen diameter (cm^2), and dp/dx is the pressure gradient along the length of the specimen.

Figure 2 plots the hydraulic conductivity for eight PW sandstone specimens under confining pressures between 3.45 MPa and 20.7 MPa. The permeability decreases from about 100×10^{-9} m/s to about 50×10^{-9} m/s as the confining pressures increase from 3.45 MPa to 20.7 MPa. The flow rates measured during unloading show a permanent reduction of the rock permeability, suggesting that a permanent closure of the pore spaces has occurred.

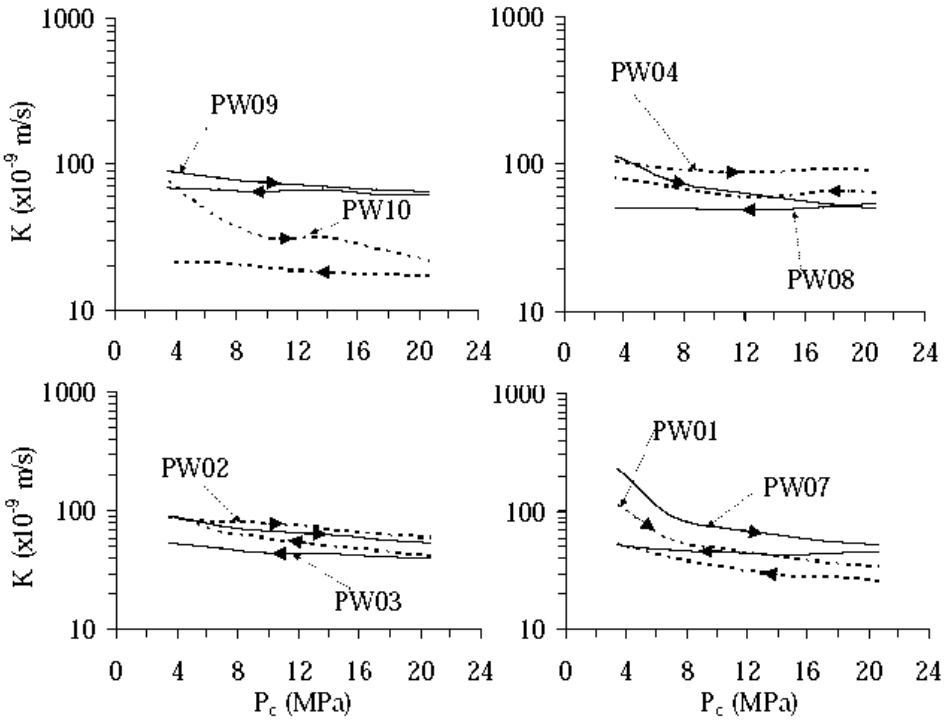

Figure 2. Hydraulic conductivity of eight PW sandstone specimens under hydrostatic stresses. Arrows indicate direction of loading and unloading.

3.2 Permeability of Intact Sandstones under Deviatoric Stresses

The laboratory arrangement for the flow testing of intact sandstone specimens under deviatoric stresses is similar to that of the testing under confining pressures. After the constant confining pressure is applied the axial stress is increased until failure occurs. The constant confining pressures varied from 1, 2, 3 to 6 MPa. The flow is measured every 6.9 MPa axial stress increment. The injected water pressure is maintained at 0.27 MPa (40 psi). A high precision pipette is used to collect the excess oil released from the triaxial cell by the specimen dilation. It will be used to calculate the volumetric strain (ε_V) of the specimen during loading:

$$\varepsilon_V = (V_O - V_S) / V_R \qquad (2)$$

where V_O is the excess oil volume, V_S is the volume of oil displaced by loading platen, and V_R is the volume of rock specimen.

Figures 3 and 4 give the permeability results for PW and PP sandstone specimens as a function of volumetric strain (ε_V). They are compared with their corresponding stress-strain curves obtained under various confining pressures (σ_3). The hydraulic conductivity is calculated by using equation (1). Before dilation the permeability of PW sandstone decreases with increasing the deviatoric stress. This agrees with the experimental by Ferfera et al. (1997), Pusch & Weber (1998), Oda et al. (2002) and Heiland (2003). The PP sandstone permeability however tends to increase with the deviatoric stresses. This may be due to error

Rock Mechanics, Fuenkajorn & Phien-wej (eds) © 2009. ISBN 978 974 533 624 7

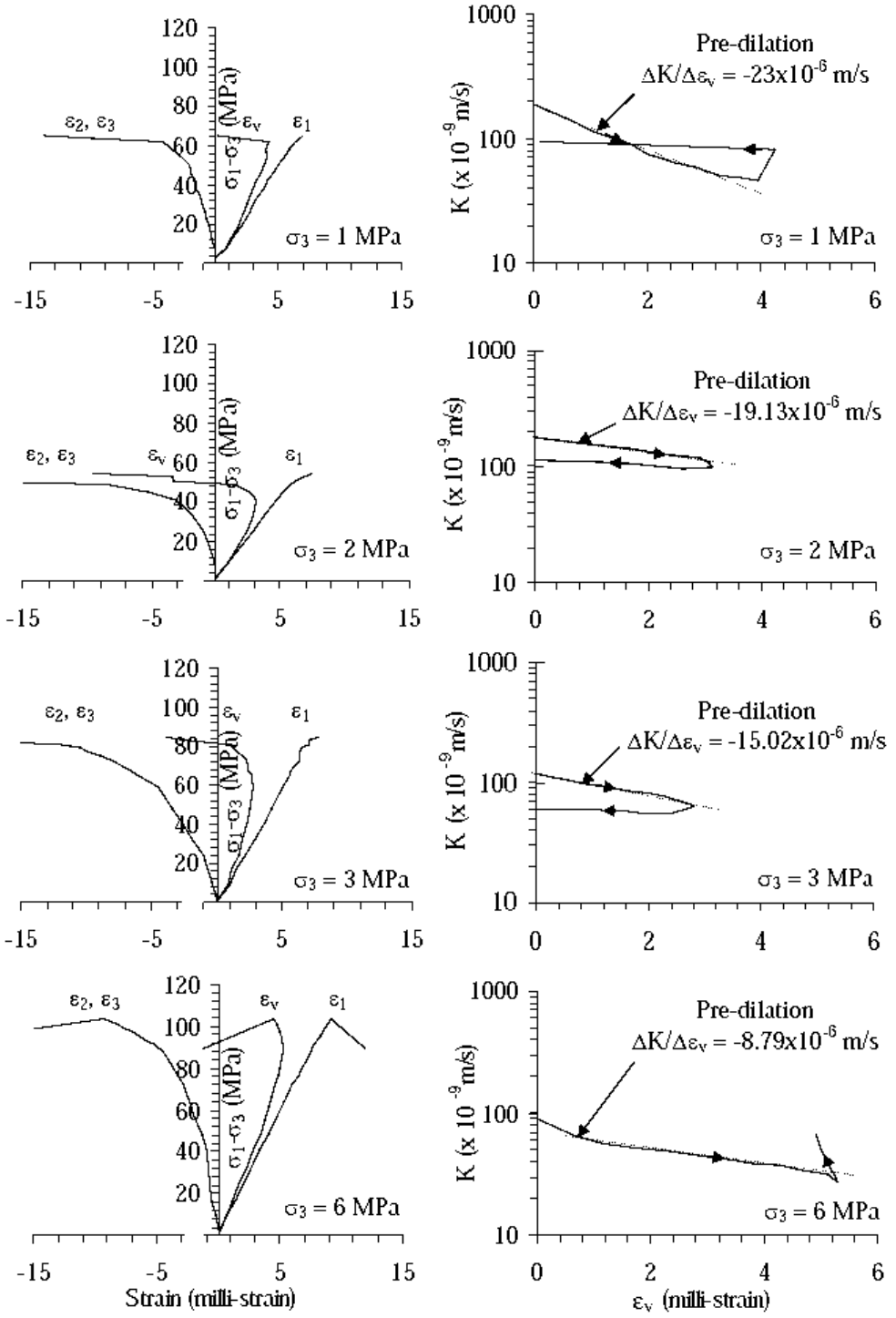

Figure 3. Permeability of PW sandstone specimens as a function of volumetric strain (ε_v) (right) and their corresponding stress-strain curves (left), for confining pressures (σ_3) from 1, 2, 3 to 6 MPa. Dotted lines represent curve fit for $\Delta K/\Delta\varepsilon_v$ ratio before failure.

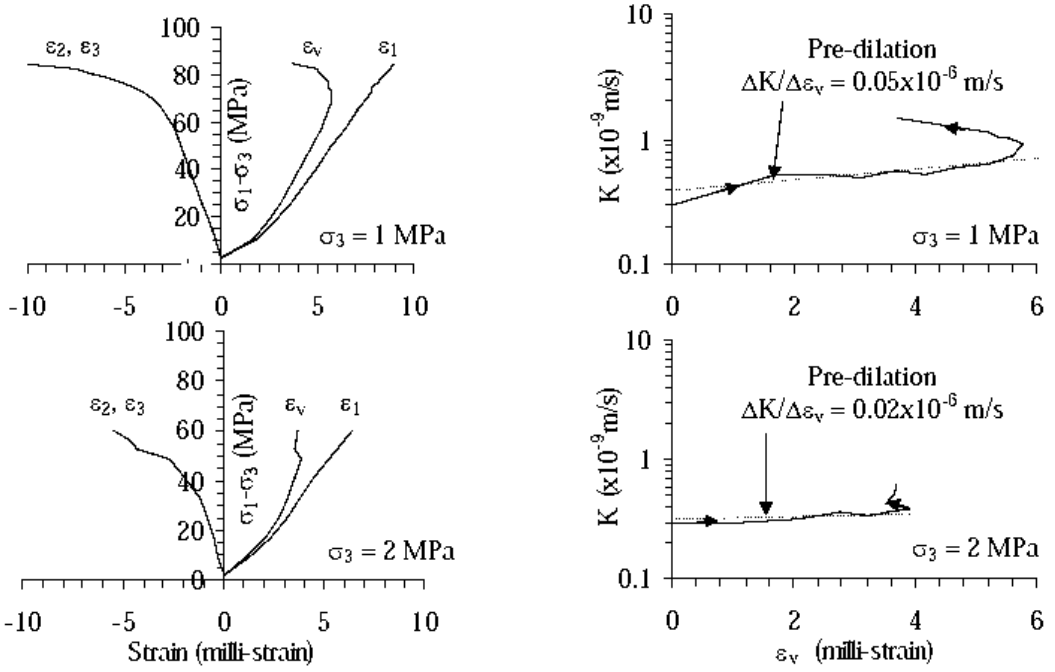

Figure 4. Permeability of PP sandstone specimens as a function of volumetric strain (ε_v) (right and their corresponding stress-strain curves (left), for confining pressures (σ_3) of and 2 MPa. Dotted lines represent curve fit for $\Delta K/\Delta\varepsilon_v$ ratio before failure.

of flow measurements. Table 2 summarizes the flow test result under deviatoric stresses. The permeability-to-volumetric strain ratio ($\Delta K/\Delta\varepsilon_V$) (before dilation strength) and the permeability-to-dilation strain ($\Delta K/\Delta\varepsilon_D$) ratio (after dilation strength) are calculated. Before dilation strength the permeability decreases with increasing volumetric strain. This is probably due to the contraction of the pore spaces in the specimen. Within this stage the $\Delta K/\Delta\varepsilon_V$ ratio decreases as increasing confining pressure. After dilation strength the rock permeability increases with specimen dilation probably because of the initiation and propagation of micro-cracks due to the applied axial stress approaching failure.

4 FLOW TESTING ON SANDSTONE FRACTURES UNDER SHEAR STRESSES

Falling head flow tests have been performed to determine the fracture permeability in sandstone specimens under shear stresses. Figure 5 shows the laboratory arrangement of the falling head flow test while the fracture is under normal and shear stresses. The maximum water head above the tested fracture is 1.23 m. The injection hole at the center of the lower block is 0.8 cm in diameter. The fractures are artificially made by applying a line load to induce a splitting tensile crack in 10×10×12 cm prismatic blocks of PW and PP sandstones (Figure 6). The fracture area is 10×10 cm. Their roughness is observed and classified by comparing with a reference profiles given by Barton (joint roughness coefficient – JRC, Barton, 1973). The constant normal stresses are 0.69, 1.38, 2.76, 3.45 and 4.14. MPa. The shear stress is applied while the shear displacement and head drop are monitored for every 0.5 mm shear displacement. The maximum shear displacement is 10 mm. The (physical) fracture aperture is measured to the nearest 0.01 mm before and after normal and shear stress application. The fracture dilations are also monitored during the shear test.

Rock Mechanics, Fuenkajorn & Phien-wej (eds) © 2009. ISBN 978 974 533 624 7

Table 2. Results of flow testing under deviatoric stresses.

	Sample No.	P_c (MPa)	E (GPa)	ν	Dilation Strength (MPa)	Ultimate Strength (MPa)	Pre-failure $\Delta k/\Delta\varepsilon_v$ ($\times 10^{-6}$ m/s)	Post-failure $\Delta k/\Delta\varepsilon_d$ ($\times 10^{-6}$ m/s)
PW	PWSS-01	1	9.31	0.23	42	65	-23.00	-3.15
	PWSS-02	2	9.14	0.25	37	55	-19.13	-3.82
	PWSS-03	3	8.52	0.33	55	88	-15.02	-4.41
	PWSS-04	6	11.98	0.29	64	103	-8.79	-100
Mean±SD					49±12	78±25		
PP	PPSS-01	1	7.89	0.31	69	85	0.05	-0.21
	PPSS-02	2	8.66	0.31	49	60	0.02	-0.21
Mean±SD					59±10	72±13		

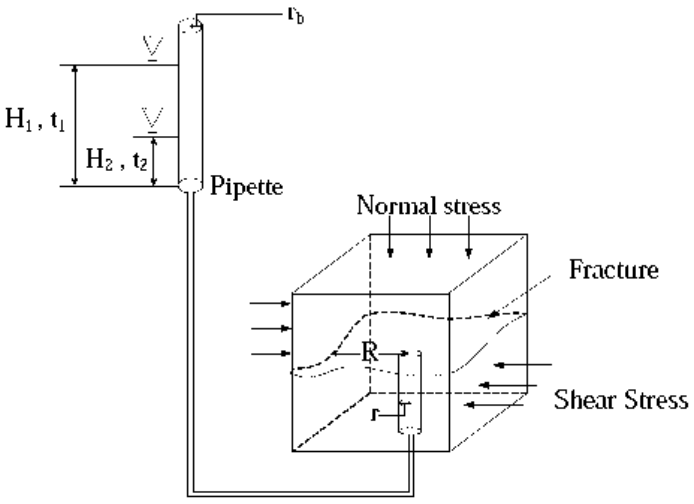

Figure 5. Laboratory arrangement for falling head test under normal and shear stresses.

The physical, mechanical and hydraulic apertures are used to calculate the hydraulic conductivity of the tested fractures. The physical aperture (e_p) is obtained from the actual measurements of the fractures before and during normal and shear stress applications. The measurement points are at the four corners of the shear box. The physical aperture at each shear displacement is an average from the four measurements. The mechanical aperture (e_m) in mm is calculated by (Barton & Bakhtar, 1983 and Bandis et al., 1983, 1985):

$$e_m = [JRC/5] / [0.2(\sigma_c/JCS) - 0.1] \quad (3)$$

where σ_c and JCS are the uniaxial compressive strength and joint compressive strength of the rock in MPa. Here σ_c and JCS are assumed to be equal.

The equivalent hydraulic aperture (e_h) for radial flow is calculated by (Maini, 1971):

$$e_h = [[\ln(H_1 / H_2) r_b^2 \ln(R / r) 6\mu] / [(t_2 - t_1)\gamma]]^{1/3} \quad (4)$$

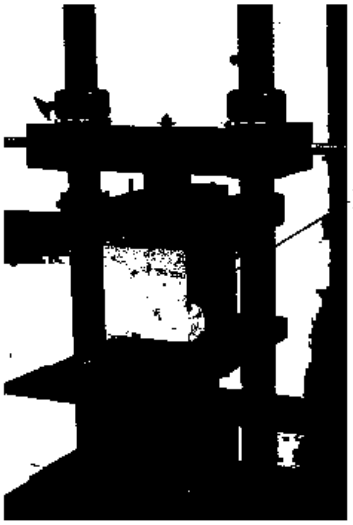

Figure 6. A 10×10×12 cm block of PW sandstone is line-loaded to induce tensile fracture in the mid-length of the block.

where γ is the unit weight of water (N/m^2), μ is the dynamic viscosity ($N \cdot s/m^2$), H_1 and H_2 are the water heads at t_1 and t_2, r_b is the pipette radius (m), R is the radius of flow path (m), and r is the radius of the radius injection hole (m).

The fracture permeability is calculated by (Zeigler, 1976):

$$K = \gamma e^2 / 12\mu \qquad (5)$$

where K represents hydraulic conductivity between smooth and parallel plates and e is the parallel plate aperture. It is assumed here that the flow is isotropic across the fracture plane, and that the intact rock is impermeable. From section 3 the intact PW sandstone permeability is about 0.1×10^{-6} m/s which is very low compared to the fracture permeability. The other sandstone permeability is less than 0.0001×10^{-6} m/s (measurement limit).

Here the fracture conductivity is calculated for three types of fracture apertures: e_p, e_m and e_h, and differentiated by different symbols as K_p – physical, K_m – mechanical, and K_h – hydraulic conductivities.

The measured JRC values range from 11, 13 to 15, which are classified as rough and undulating; bedding and tectonic joints; and relief joints, respectively. From equation (3) the equivalent mechanical apertures for the above JRC values are 220, 260 and 300 micro-meters.

The fracture hydraulic conductivities are calculated for the three aperture measurements and plotted as a function of shear displacement (u) for normal stresses of 0.69, 2.75 and 4.14 MPa in Figures 7 and 8 for PW and PP sandstones. They are also compared with their corresponding shear stress-shear displacement diagram. Since the shear stresses after the peak value remain relatively consistent through 10 mm of displacement, up to 3 mm shear displacement is plotted in the figures.

Rock Mechanics, Fuenkajorn & Phien-wej (eds) © 2009. ISBN 978 974 533 624 7

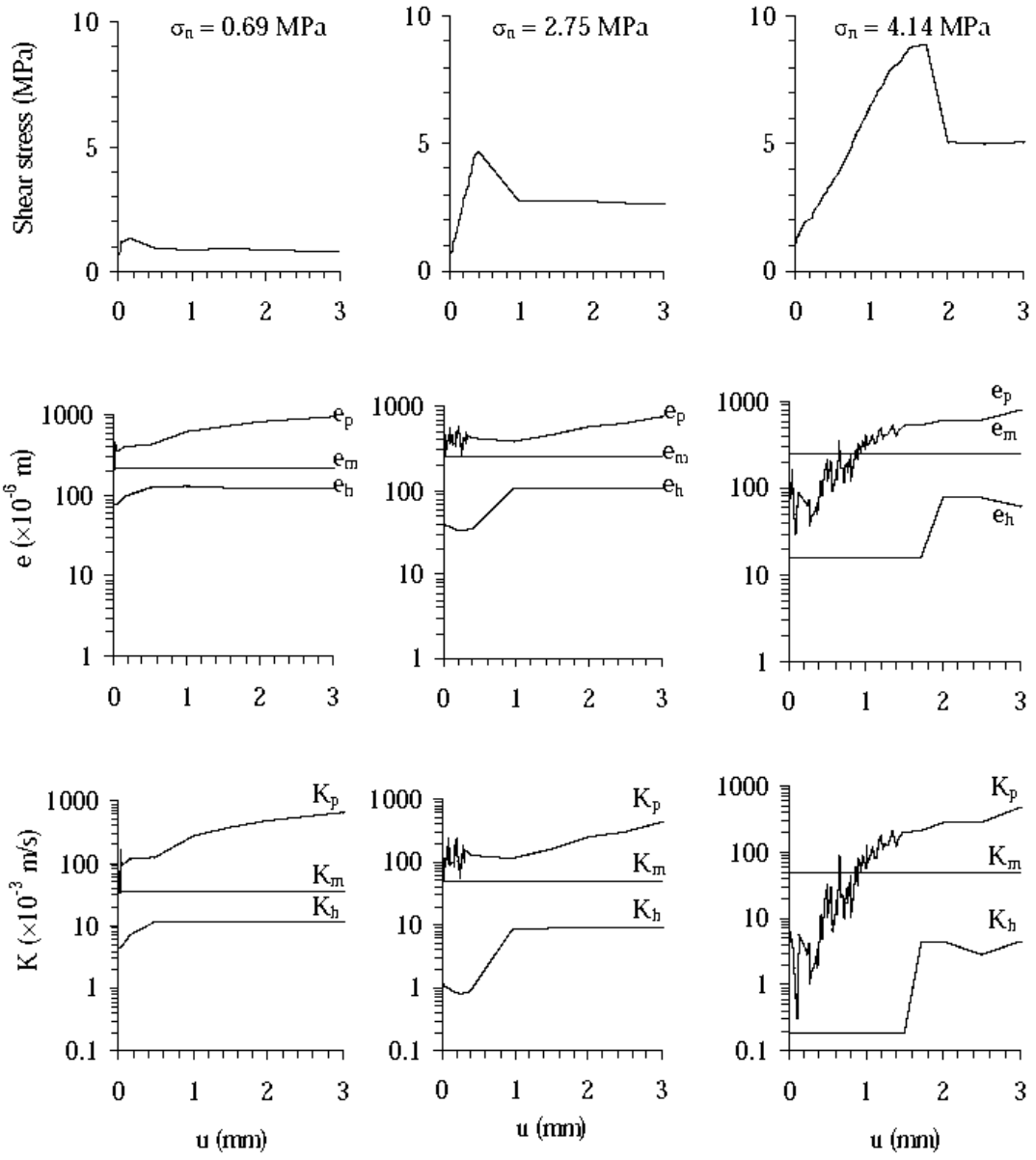

Figure 7. Shear stress, fracture aperture and hydraulic conductivity as a function of shear displacement (u) for PW sandstone fractures under normal stresses of 0.69 MPa (left), 2.75 MPa (middle) and 4.14 MPa (right).

Observations of pre– and post–test fracture areas suggest that no significant change has occurred in terms of fracture roughness. Even though some portion of fracture is sheared off the JRC's remain roughly the same. This is primarily because the applied normal stresses are relatively low. The mechanical aperture, e_m before, during and after shearing therefore remains constant during the shearing process. As a result the hydraulic conductivity K_m calculated from e_m is independent of the shearing displacement. An example of the post–test fracture for PW sandstone is shown in Figure 9.

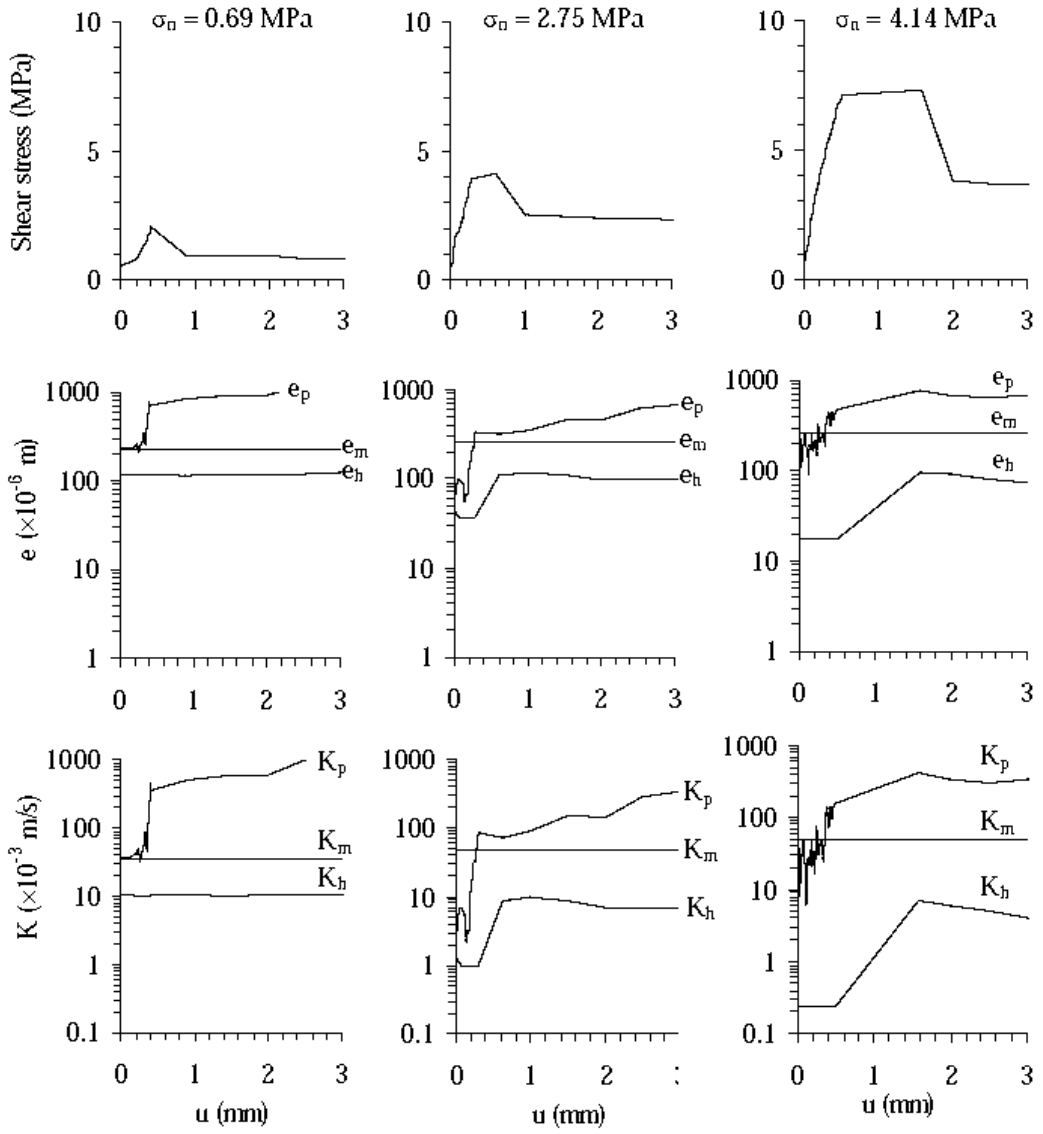

Figure 8. Shear stress, fracture aperture and hydraulic conductivity as a function of shear displacement (u) for PP sandstone fractures under normal stresses of 0.69 MPa (left), 2.75 MPa (middle) and 4.14 MPa (right).

For both PW and PP sandstones the physical aperture e_p tends to increase with shearing displacement. Its value fluctuates before the peak and tends to be more consistent in the residual stress region. The K_p values calculated from e_p subsequently show similar characteristics of the curves in the permeability-shear displacement diagram.

The hydraulic aperture e_h indirectly determined from the inflow rates also tends to increase with the shear displacement, particularly under high normal stresses. Even though K_p and K_h show similar characteristics of the curves in the permeability-shear displacement diagram, K_p is always about an order of magnitude greater than K_h, particularly in the residual shear region.

Rock Mechanics, Fuenkajorn & Phien-wej (eds) © 2009. ISBN 978 974 533 624 7

Figure 9. Example of post-test fracture surfaces in a PW sandstone specimen. The sheared surfaces are indicated by white areas.

Figures 10 and 11 plot the hydraulic conductivity derived from e_h as a function of normal stress σ_n. The fracture permeability values under no shear stress, immediately before the peak stress, and under the residual shear stress are compared. The fracture permeability under residual shear region is greater than that under no shear and that immediately before peak stress. It is not very sensitive to the normal stress – showing a slightly decrease with increasing the normal stress. The magnitudes of fracture permeability under no shear and under peak stress are similar. Both tend to decrease exponentially with the normal stress. As a result the difference between the permeability under residual shear stress and that under peak stress becomes larger as the normal stress increases. The results agree reasonably well with those obtained by Lee & Cho (2002) and Son et al. (2004).

This suggests that under a given normal stress, the fracture permeability immediately before peak stress will remain similar to that under no shear stress. After the fracture is displaced beyond the peak stress its permeability will however notably increase particularly under high normal stresses. The change of the fracture permeability with the normal stress will be presented in the next section.

From the shear stress-displacement diagrams as shown in Figures 7 and 8, the joint shear stiffness for various normal stresses has been calculated at the 50% peak stress using an equation (Indraratna & Ranjith, 2001):

$$k_s = \tau_s/\delta_s \quad (6)$$

where k_s is the joint shear stiffness (MPa/m), τ_s is the shear stress (MPa), δ_s is the shear displacement (m). Table 3 summarizes the results for PW and PP sandstones. The joint shear stiffness tends to increase with the normal stresses.

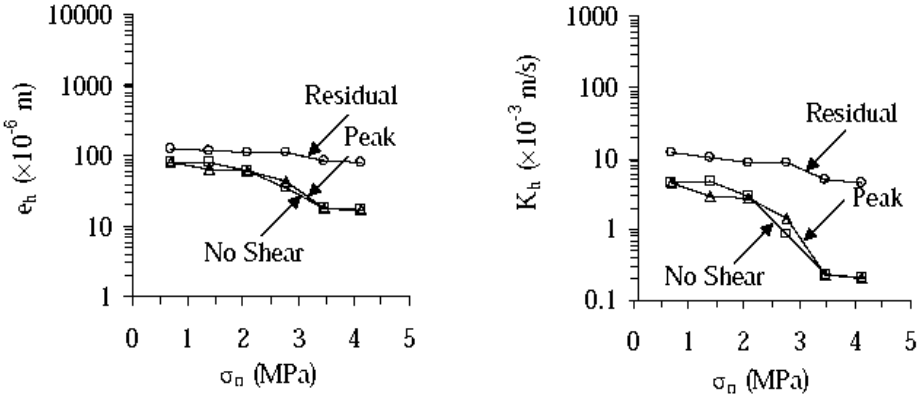

Figure 10. Hydraulic aperture (left) and hydraulic conductivity (right) as a function of applied normal stress for PW sandstone specimens.

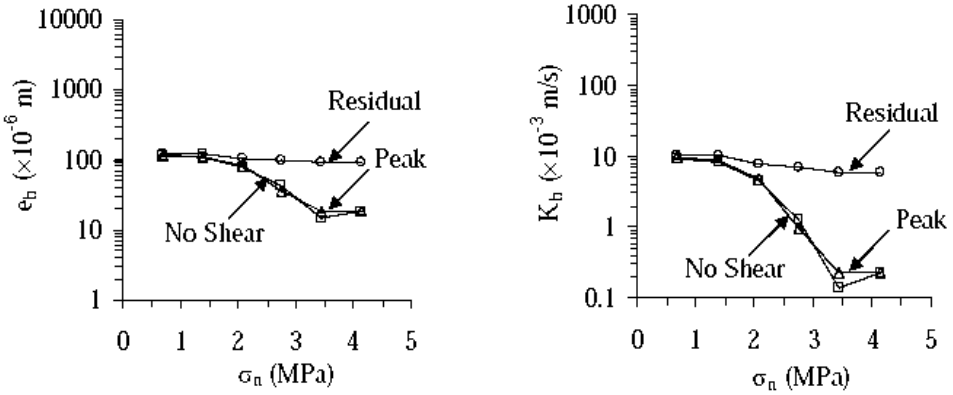

Figure 11. Hydraulic aperture (left) and hydraulic conductivity (right) as a function of applied normal stress for PP sandstone specimens.

Table 3. Joint shear stiffness for PP and PW sandstones.

PP	K_s(GPa/m)	PW	K_s(GPa/m)
PPSS-DS-01	5.17	PWSS-DS-01	11.49
PPSS-DS-02	6.47	PWSS-DS-02	12.93
PPSS-DS-03	11.34	PWSS-DS-03	10.34
PPSS-DS-04	14.13	PWSS-DS-04	8.08
PPSS-DS-05	8.62	PWSS-DS-05	6.47
PPSS-DS-06	9.42	PWSS-DS-06	6.90
Average	9.19±3.25	Average	9.37±2.62

5 FLOW TESTING ON SANDSTONE FRACTURES UNDER NORMAL STRESSES

Falling head flow tests have been performed to determine the fracture permeability in PW, PP, PK and SK sandstone specimens under normal stresses. One cycle of loading and unloading has been made during the flow test. During loading the normal stresses are

Rock Mechanics, Fuenkajorn & Phien-wej (eds) © 2009. ISBN 978 974 533 624 7

progressively increased from 0.35, 0.69, 1.03, 1.39, 1.72 to 2.06 MPa. During unloading the normal stresses are reduced from the maximum to the minimum while the flow rates are continuously measured. The tested fractures are tension-induced fractures with a nominal area of 15×15 cm. The flow test arrangement is similar to the flow test under shear stresses. A minimum of 3 specimens have been tested for each sandstone type.

The hydraulic aperture e_h and hydraulic conductivity K_h of the fractures are plotted as a function of the normal stress in Figure 12. They are calculated by using equations (4) and (6). For all sandstone types the fracture hydraulic conductivities exponentially decrease with increasing the normal stresses. Their permeability is in the range between 100×10^{-6} m/s and 10000×10^{-6} m/s. A permanent fracture closure is usually observed after unloading as evidenced by the permanent reduction of the fracture permeability (flow rate). The joint normal stiffness is calculated by an equation (Indraratna & Ranjith, 2001):

$$k_n=\sigma_n/\delta_n \tag{7}$$

where k_n is the joint normal stiffness (MPa/m), σ_n is the normal stress (MPa), δ_n is the joint deformation or closure (m). Table 4 summarizes the results. Due to the permanent closure of the fracture under the normal stresses the normal stiffness determined from the loading curves is significantly less than that from the unloading curves.

6 DISCUSSIONS AND CONCLUSIONS

The hydraulic conductivities of the intact PW and PP sandstones decreases with increasing volumetric strain before dilation strength probably due to the closure of voids and micro-cracks, and increases with the dilation strain after the dilation strength due to the initiation and propagation of cracks and fractures. The hydraulic conductivity of the PW sandstone decreases from about 100×10^{-9} m/s to about 50×10^{-9} m/s as the confining pressures increase from 3.45 MPa to 20.7 MPa. The flow rates measured during unloading show a permanent reduction of the rock permeability, suggesting that a permanent collapse of the pore spaces has occurred.

Both physical and hydraulic apertures (e_p and e_h) increase with shearing displacement, particularly under high normal stresses. The hydraulic conductivity derived from the actual aperture measurement (K_p) is about an order of magnitude greater than that indirectly determined from the flow rate (K_h), particularly in the residual shear region. The magnitudes of fracture permeability under no shear and under peak stress are similar. The K_h values in the residual shear region are greater than that immediately before peak stress. Both tend to decrease exponentially with the normal stress. The difference between the permeability under residual shear stress and that under peak stress becomes larger as the normal stress increases. For all sandstones tested here the fracture hydraulic conductivities exponentially decrease with increasing the normal stresses. Their permeability is in the range between 100×10^{-6} m/s and 10000×10^{-6} m/s. A permanent fracture closure is usually observed after unloading as evidenced by the permanent reduction of the flow rate.

More testing is required to develop mathematical relationships between the fracture hydraulic conductivity (or hydraulic apertures) with the applied normal stresses for the peak and the residual regions. Such relations would be useful in predicting the fracture permeability in rock mass around underground excavations or in the slope embankments where displacement of fractures usually occur.

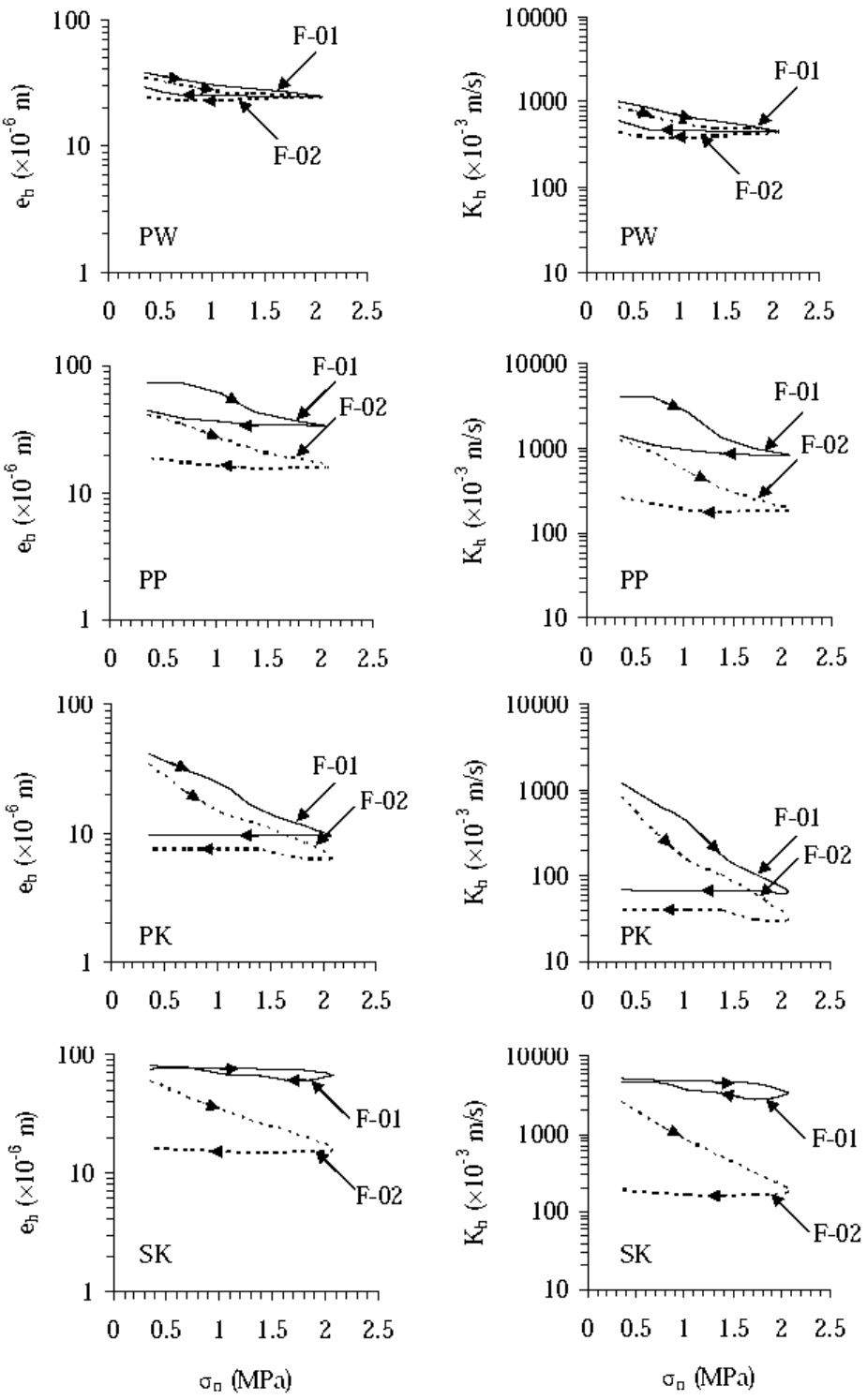

Figure 12. Hydraulic aperture (e_h) and hydraulic conductivity (K_h) as a function of normal stress (σ_n) for fracture in PW, PP, PK and SK sandstones.

Rock Mechanics, Fuenkajorn & Phien-wej (eds) © 2009. ISBN 978 974 533 624 7

Table 4. Joint normal stiffness for PW, PP, PK and SK sandstones.

K_n (GPa/m)	PW	PP	PK	SK
Loading	427.2±533.7	85.2±43.2	72.3±45.1	48.5±20.3
Unloading	1548.9±1817.4	1837.9±3875.5	18504.3±4296.8	211±905.9

ACKNOWLEDGTMENT

This research is funded by Suranaree University of Technology. Permission to publish this paper is gratefully acknowledged.

REFERENCES

Auradou, A., Drazer, G., Boschan, A., Hulin, J.P. & Koplik, J., 2006. Flow channeling in a single fracture induced by shear displacement. *Geothermics*. 35(5-6): 576–588.

Baghbanan, A. & Jing, L., 2008. Stress effects on permeability in a fractured rock mass with correlated fracture length and aperture. *International Journal of Rock Mechanics & Mining Sciences*. 45(8): 1320-1334.

Bandis, S.C., Barton, N.R. & Christianson, M., 1985. Application of a new numerical model of joint behaviour to rock mechanics problems. *Proc. Int. Symps. On Fundamentals of Rock Joints*, Bjorkliden.

Bandis, S.C., Lumsden, A.C. & Barton, N.R., 1983. Fundamentals of rock joint deformation. *Int. J. Rock Mech. Min. Sci. Geomech. Abstr*. 20: 249-268.

Barton, N. & Bakhtar, K., 1983. Rock joint description and modeling for the hydrothermomechanical design of nuclear waste repositories (Contract Report, submitted to CANMET). *Mining Research Laboratory*, Ottawa, Parts 1-4: 270; Part 5: 105.

Ferfera, F.M.R., Sarda, J-P., Bouteca, M. & Vincke, O., 1997. Experimental study of monophasic permeability changes under various stress paths. *Int. J. Rock Mech. & Min. Sci*. 34: 3-4.

Heiland, J., 2003. Permeability of triaxially compressed sandstone: Influence of deformation and strain-rate on permeability. *Pure appl. Geophys*. 160: 889-908.

Indraratna, B. & Ranjith, P.G., 2001. Laboratory measurement of two-phase flow parameters in rock joints based on high pressure triaxial testing. *Journal of Geotechnical and Geoenvironmental Engineering*. 127(6): 530-542.

Indraratna, B., & Ranjith, P., 2001. *Hydromechanical Aspects and Unsaturated Flow in Joints Rock*. Lisse: A. A. Balkema.

Iscan, A.G., Kok, M.V., & Bagc, A.S., 2006. Estimation of permeability ans rock mechanical properties of limestone reservoir rocks under stress conditions by strain gauge. *Journal of Petroleum Science and Engineering*. 53: 13-24.

Lee, H. S. & Cho, T.F., 2002. Hydraulic characteristics of rough fractures in linear flow under normal and shear load. *Rock Mechanics and Rock Engineering*. Springer-Verlag Wien. 35(4): 299-318.

Maini, Y.N.T., 1971. *In situ hydraulic parameters in jointed rock-their measurement and interpretation*. Ph.D. Thesis. Imperial College, London. 321 p.

Niemi, A.P., Vaittinen, T.A., Vuopio, J.A. & Polla, J.P., 1997. Simulation of heterogeneous flow in a natural fracture under varying normal stress. *International of Rock Mechanics and Mining Sciences*. 34(3-4): 565.

Oda, M., Takemura, T., & Aoki, T., 2002. Damage growth and permeability change in triaxial compression tests of Inada granite. *Mechanics of Materials 34 (2002)* 313–331.

Pusch, G. & Weber, J.R., 1998. Correlation of rock permeability and anisotropic stress conditions for the integration of rock mechanical and hydraulic flow models. *SCA Paper 9826.*

Pyrak-Noltea, L.J. & Morrisa, J.P., 2000. Single fractures under normal stress: The relation between fracture specific stiffness and fluid flow. *International Journal of Rock Mechanics and Mining Sciences.* 37(1): 245-262.

Shangxian, Y. & Shangxu W., 2006. Effect and mechanism of stresses on rock permeability at different scales. *Science in China: Series D Earth Sciences 2006.* 49(7): 714-723.

Son, B. K., Lee, Y. K. & Lee, C.I., 2004. Elasto-plastic simulation of a direct shear test on rough rock joints. *International Journal of Rock Mechanics & Mining Sciences.* 41: 1-6.

Xiao, Y.X., Lee, C.F. & Wang, S.J., 1999. Assessment of an equivalent porous medium for coupled stress and fluid flow in fractured rock. *International of Rock Mechanics and Mining Sciences.* 36(7): 871-881.

Zeigler, B. 1976. *Theory of Modelling and Simulation.* New York: John Wiley and Sons.

Zhou, J. J. & Shao, J. F., 2006. micromechanical study of damage growth and permeability variation in brittle rocks. *Studia Geotechnica et Mechanica.* Vol. 28, No. 1, 2006.

Zhu, W., Montési, Laurent G. J. & Wong, T.F., 2002. Effects of stress on the anisotropic development of permeability during mechanical compaction of porous sandstones. *Geological Society, London, Special Publications*; 2002; v. 200; p. 119-136.

.

BIOGRAPHY

Mr. Panupong Suanprom was born on February 28, 1985 in Nakhonratchasima province, Thailand. He received his Bachelor's Degree in Engineering (Geotechnology) from Suranaree University of Technology in 2006. For his post-graduate, he continued to study with a Master's degree in the Geological Engineering Program, Institute of Engineering, Suranaree university of Technology. During graduation, 2006-2009, he was a part time worker in position of research assistant at the Geomechanics Research Unit, Institute of Engineering, Suranaree University of Technology. He published technical paper related to rock mechanics, titled **"Permeability Testing of Sheared Fractures in Sandstones"** in the Proceedings of the Second Thailand Symposium on Rock Mechanics, Chonburi, Thailand.